A STUDY OF CURRENT METER OBSERVATIONS OF THE SEMIDIURNAL BAROCLINIC TIDE OF THE WESTERN NORTH ATLANTIC

by

RONALD R. REGAL

B.A., Wabash College
(1970)

SUBMITTED IN
PARTIAL FULFILLMENT
OF THE REQUIREMENTS FOR THE
DEGREE OF MASTER OF SCIENCE

at the

MASSACHUSETTS INSTITUTE OF TECHNOLOGY
February, 1972

Signature of Author .....
Department of
Earth and Planetary Sciences
January 21, 1972

Certified by .....
Thesis Supervisor

Accepted by .....
Chairman, Departmental Committee
on Graduate Students

A Study of Current Meter Observations of the Semidiurnal Baroclinic Tide of the Western North Atlantic

by
Ronald Ray Regal

Submitted to the Department of Earth and Planetary Sciences on January 21, 1972, in partial fulfillment of the requirements for the degree of Master of Science.

ABSTRACT

The Fourier coefficients of east and north horizontal water velocity in 58 moored current meter records from the western North Atlantic were inspected for the presence of internal tides. The M_2 internal tide was found to be the dominant and most frequent of the internal tides but still showed great variability. Four measures of the M_2 internal tide were shown - Fourier coefficients, admittances, tidal ellipses, and power densities. All showed a tendency for M_2 internal tidal amplitudes to decrease with increasing depth. The variation with depth of the M_2 power density was found to resemble that of the Brunt-Vaisala frequency, indicating baroclinic modes of internal gravity waves. The part of the M_2 internal tide attributable to the barotropic, surface tide was found to be relatively small. Semidiurnal east velocities at Site D (39°20'N, 70°W) were generally larger than north velocities, especially in deep records, possibly indicating interaction with the continental shelf to the north of Site D.

Thesis Supervisor: Carl Wunsch

Title: Associate Professor of Oceanography

ACKNOWLEDGEMENTS

The author wishes to sincerely thank Dr. Carl Wunsch for the guidance and ideas that made this study possible. Without his thinking and readiness to discuss the work, this paper could have never been. The author especially wants to thank Dr. Wunsch for the encouragement to put this study into its present form.

Thanks is also given to Dr. William Schmitz for the data, help, and a place to work in Woods Hole.

This work was supported by the National Science Foundation under contract GA13880.

TABLE OF CONTENTS

LIST OF TABLES AND FIGURES

TABLES

FIGURES

I. INTRODUCTION

The importance of the rythmic rise and fall of the sea surface known as the tide has been recognized for many years, and study of tides has been rewarded with considerable knowledge. Only more recently have motions within the ocean of tidal period attracted much attention, and understanding of these internal tides is still in the formulative stage. The internal tides are attracting attention now not only as an interesting phenomenon with many unanswered questions but also as a possibly important part of energy flows in the ocean.

As is well known, the tide is intimately connected with the motions of the moon and sun relative to the earth. The not quite twice daily rise and fall of the tide in most places reflects the 12.42 hours the moon takes to go halfway around the rotating earth. The part of the tide which a cosine wave of period 12.42 hours is called the M_2 tide. The tidal forcing of the sun and moon is not one simple cosine, so other periods are present in the tides. The principal semidiurnal and diurnal components of the tidal generating force are shown in Table 1 (DEFANT, 1958). In measurements of currents and internal temperatures these same periodicities sometimes appear. These internal motions of tidal

TABLE 1

MAJOR TIDAL FORCING PERIODS
(Defant, 1958)

	SYMBOL	PERIOD (Hours)	AMPLITUDE (Relative)	DESCRIPTION
Semidiurnal tides	M_2	12.42	100.0	Main lunar (semi-diurnal) constituent.
	S_2	12.00	46.6	Main solar (semi-diurnal) constituent.
	N_2	12.66	19.1	Lunar constituent due to monthly variation in moon's distance.
	K_2	11.97	12.7	Soli-lunar constituent due to changes in declination of sun and moon.
Diurnal tides	K_1	23.93	58.4	Soli-lunar constituent.
	O_1	25.82	41.5	Main lunar (diurnal) constituent.
	P_1	24.07	19.3	Main solar (diurnal) constituent.

periods are known as internal tides.

Semidiurnal internal fluctuations have been found in the ocean by many observers. Some recent observations include those of Doebler (1967), Hecht and Hughes (1971), Isaacs (1966), Lee and Cox (1966), Niiler (1968), Nowroozi (1968), Sabinin and Shulepov (1970), and Wunsch and Dahlen (1970). These include temperature and current measurements in shallow and deep water. Most of the internal tides observed have been semidiurnal. Even when present, the diurnal internal tides are usually less significant than the semidiurnal. Many times the semi-diurnal internal tide is the most significant fluctuation in the record, but often the record is dominated by large inertial oscillations, which have been more extensively studied than the tidal period oscillations.

Defant (1950) stated that internal tides are as common as surface tides, but further observations have shown that although common, internal tides are by no means found everywhere all the time. Sabinin and Shulepov (1970) set up two temperature sensing arrays in the tropical Atlantic - one north and one south of the Mid-Atlantic Ridge, which runs east-west near the equator. They found definite semidiurnal oscillations at all levels and moorings in the northern area,but in the southern area semidiurnal fluctuations could barely be seen above the

background. Even more curiously, semidiurnal internal tides come and go at the same place. Hecht and Hughes (1971) maintained a temperature sensing mooring on the top 100 meters at 45°56'N, 08°19'W in the Bay of Biscay for seven days in late November 1967 and again for four days eleven days later. The first records showed significant semidiurnal peaks at all levels; the second had none at any level.

That internal tides seem to be intermittent suggests that the internal tide is not simply an undersea manifestation of the surface tide, and further evidence confirms this. For one, vertical motions seen in temperature measurements can be many times greater than equilibrium tidal heights. Lee and Cox (1966) found semidiurnal vertical fluctuations of ten meters off the coast of California compared to an equilibrium tidal height of 0.4 meters for M_2 at 30° N. They note that although waves of far higher amplitude than equilibrium value could be generated by resonance in an inviscid fluid, this would require inadmissibly low damping. Being in the class of long waves, the surface tide should induce vertical displacements which decrease linearly from surface to bottom, but investigators including Hecht and Hughes (1971) and Lee and Cox (1966) have found greatest semidiurnal vertical displacements below the

surface.

Although large vertical displacements at mid-depths disqualify internal semidiurnal tides from being just part of the surface tide, such behavior is characteristic of non-zero mode internal gravity waves. Fofonoff (1969) showed that fluctuations with frequencies between the local inertial and maximum Brunt-Vaisala frequencies tend to be governed by internal wave dynamics. The inertial frequency, $\sin\theta/12$ cycles/hour where θ = latitude, will be less than 1/12.42 cycles/hour, the M_2 frequency, for all except extreme polar regions. The Brunt-Vaisala frequency depends on the stratification in such a way that in most oceanic situations the maximum Brunt-Vaisala frequency in the water column is greater than the M_2 frequency. So in most oceanic situations, semidiurnal fluctuations are in the frequency range governed by internal wave dynamics. The surface tide is a mode zero internal wave, the barotropic tide. Part of any internal tide will be barotropic, but observed semidiurnal tides have tended to be at least in large part composed of non-zero modes. The non-barotropic part of the internal tide is called the baroclinic tide.

Although it is fairly certain that the internal tides are internal waves, their distribution and origin are still uncertain. The general feeling is that semi-

diurnal internal tides must be generated by the interaction of the surface tide with bottom topography. Currently the two most prominent theories as to how this happens belong to Cox and Sandstrom (1962) and Rattray (1960 and 1969). Cox and Sandstrom have the surface tide interacting with a rough bottom, whereas Rattray's surface tide meets a steplike continental shelf, sending internal tides seaward normal to the coastline. Hecht and Hughes (1971) said it is widely accepted that the internal tides are generated by the incidence of the surface tide on the continental shelf, but any acceptance Rattray's model has comes from a feeling that the model is too good not to be true rather than from observational proof.

Hecht and Hughes (1971) themselves were unable to make Rattray's model fit their data nearly as well as they would have liked. They could explain part of the shrinking of the semidiurnal oscillations between the two trips by the incidence of spring and neap tides on the coast but had to figure oceanic conditions had changed in such a way as to be less favorable to the generation and propogation of semidiurnal internal waves. In their 1969 paper Rattray et al. show that with constant Brunt-Vaisala frequency, consideration of many modes confines the strong motion in their model to

within rays emanating from the corner of the shelf. These rays travel parallel to the group velocity, that is at a slope of $[(\omega^2-f^2)/(N^2-\omega^2)]^{1/2}$, where ω is the frequency of the wave and N and f are the appropriate Brunt-Vaisala frequencies. Hecht and Hughes (1971) give a value of N = .1 cycles/minute, and for them $f \cong .5/12$ cycles/hour and $\omega \cong 1/12$ cycles/hour. These values give a slope of about .01. This is a shallow slope to the eye but becomes considerable on oceanic scales. The continental shelf nearest Hecht and Hughes' station is 200 kilometers away toward Brest, France, or Coruna, Spain. A ray starting from the edge of the nearest shelf and travelling at a slope of .01 would hit Hecht and Hughes' mooring at about 2000 meters below the surface. Hecht and Hughes, though, were in the top 100 meters. Rattray et al. (1969) mention that Le Blond (1966) found higher modes in internal waves to be more rapidly damped than lower modes,so the internal tides will gradually lose their beamlike appearance and become more widely spread in the vertical. With a non-constant Brunt-Vaisala frequency Rattray et al. (1969) indicate that a refraction ot the beams takes place with the beams still intact. Presumedly then, lower Brunt-Vaisala frequencies in the lower layers of the Bay of Biscay would tend to increase the slope and make the rays dive deeper yet. So although Rattray's model looks good

and internal tides may well be generated at the edges of the continental shelves, it may be dangerous to think of simple rays as more than a first cut at a picture of internal tides in the ocean. Even if Rattray's model does prove to be correct, this would not necessarily disprove the Cox and Sandstrom (1962) model. Sabinin and Shulepov (1970) thought they saw evidences of semidiurnal internal tides generated at the Mid-Atlantic Ridge, so all internal tides may not be generated at the continental shelves.

If the surface tide is converted partially into internal tides, possibly along all coastal areas, some interesting possibilities are raised. If a substantial part of the energy dissapated tidally by the sun and moon (about 3×10^{19} ergs/second) goes into the internal tides rather than into the shallow seas as heat, then the internal tides become an important consideration in an understanding of energy in the oceans (WUNSCH, 1971). A chain of energy flow from the surface tide through the internal tides to other parts of the spectrum might account for large energies found at great depths and large observed inertial oscillations (WUNSCH, 1971). Hecht and Hughes (1971) found high frequency basic internal waves only in the presense of semidiurnal oscillations, which may indicate an exodus of tidal energy to other frequencies. By introducing significant vertical

and horizontal velocities into the water column, internal tides become a possibly important source of oceanic mixing (WUNSCH, 1971).

Internal tides, then, are a not well-understood, possibly important phenomenon in the ocean. Dr. Wunsch thought the current meter records gathered by the Buoy Group under the direction of N.P. Fofonoff and T.F. Webster at the Woods Hole Oceanographic Institution might yield valuable information on the internal tides. This study is a look at the internal tides in many of the longer Buoy Group records.

II. FOURIER COEFFICIENTS

The data used for this study are the Fourier coefficients for horizontal current measurements. The current measurements were made by the Buoy Group at the Woods Hole Oceanographic Institution between 1965 and 1970 with Richardson type current meters (RICHARDSON, STIMSON, and WILKINS, 1963). Most of the measurements were taken at Site D which is at roughly 39°20'N, 70°W in about 2600 meters of water. This puts Site D about 50 kilometers south of the bottom of the continental slope and 175 kilometers north of the approximate mean axis of the Gulf Stream (WEBSTER, 1969). The location of Site D is shown in Figure 1 (WEBSTER, 1969). The other measurements were taken either farther south in deeper water or to the north of Site D near the continental shelf. The locations and times of the records used are given in Table 2. The numbering of the records is that used by the Buoy Group. The first three digits refer to the mooring, and the last digit is the position of the meter on the mooring. For instance record 1892 came from the second shallowest meter on mooring 189. The shallowest was not used here. Varieties of film and magnetic tape meters were used during the six year span, but the basic method of sampling was to take burst samples at uniform intervals,

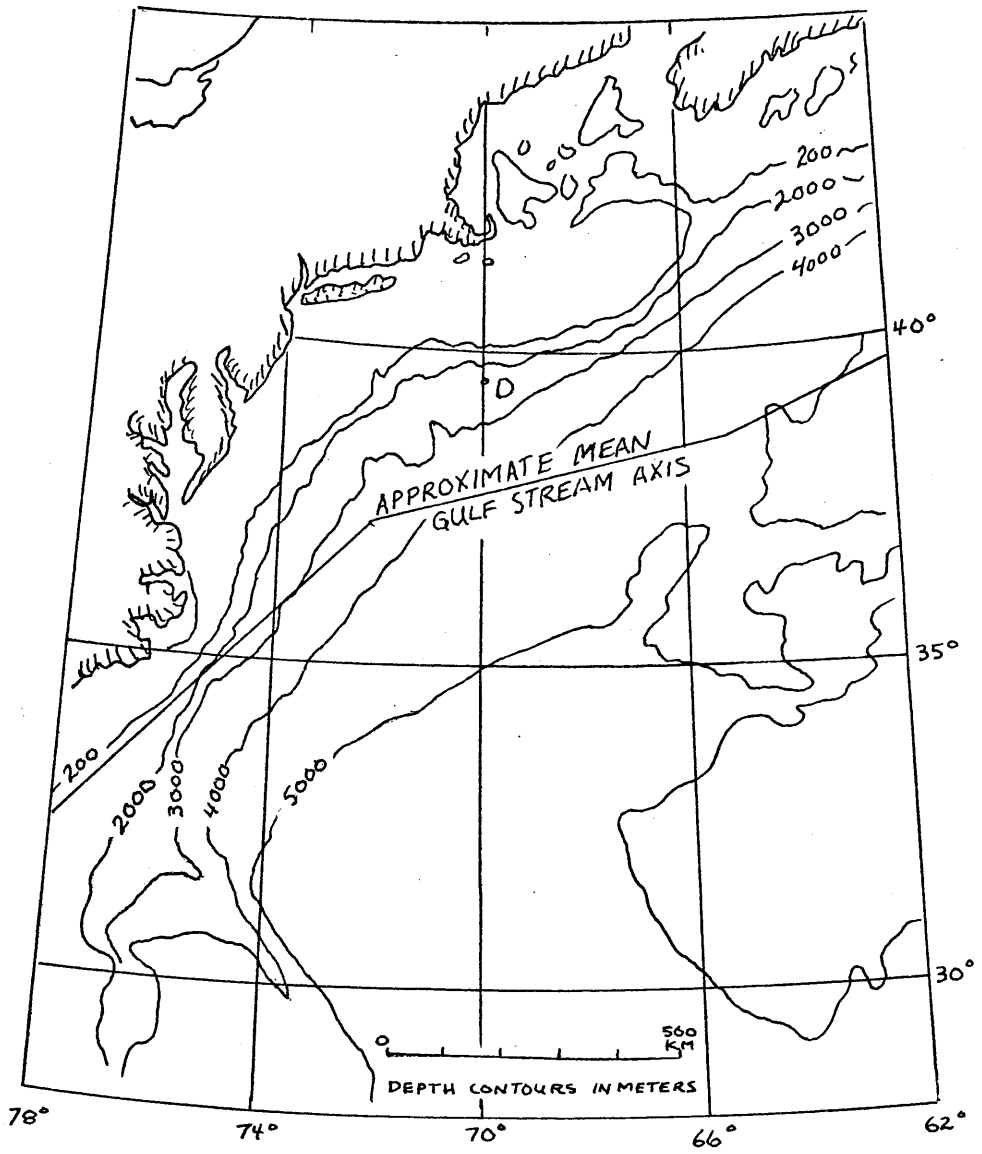

FIGURE 1
POSITION OF SITE D (WEBSTER, 1969)

TABLE 2

CURRENT METER RECORDS

RECORD	LAT. N	LONG. W	DEPTH m.	START TIME GMT	START DATE	STOP TIME GMT	STOP DATE
1892	39°20.0'	69°57.0'	99	0006	7 Oct 65	1406	20 Nov 65
1894	"	"	1001	0008	7 Oct 65	1808	11 Nov 65
1895	"	"	2002	0008	7 Oct 65	0208	26 Nov 65
1932	39°19.0'	70°00.0'	492	1236	7 Feb 66	2036	28 Mar 66
1933	"	"	994	1253	7 Feb 66	0853	30 Mar 66
2121	39°20.0'	69°51.5'	50	1826	8 Oct 66	0826	7 Dec 66
2124	"	"	950	1823	8 Oct 66	1223	7 Dec 66
2125	"	"	1950	1822	8 Oct 66	0022	18 Nov 66
2203	39°17.9'	70°05.6'	106	0013	27 Feb 67	2213	11 Apr 67
2204	"	"	511	0010	27 Feb 67	0810	13 Apr 67
2205	"	"	1013	0012	27 Feb 67	2121	14 Apr 67
2651	39°10.9'	69°55.0'	2578	0023	25 Apr 68	0823	15 Jun 68
2681	39°09.7'	69°51.7'	2671	0803	16 Jun 68	2003	20 Sep 68
2743	39°10.2'	70°04.2'	54	1508	22 Aug 68	2308	2 Oct 68
2843	39°09.8'	70°03.6'	54	2345	19 Dec 68	1345	7 Mar 69
2871	39°10.7'	70°02.1'	2580	2339	19 Dec 68	0539	31 Jan 69
2983	39°09.1'	69°59.0'	14	0044	28 Apr 69	0044	10 Aug 69
3021	39°05.9'	69°59.5'	2586	1933	8 Jun 69	1533	11 Oct 69
3041	36°23.4'	70°00.2'	4287	2148	12 Jun 69	0148	14 Aug 69
3051	36°43.0'	70°00.3'	4227	2018	12 Jun 69	0218	14 Aug 69
3093	39°09.0'	70°02.0'	13	0107	14 Jun 69	2307	10 Aug 69
3095	"	"	56	2220	13 Jun 69	1820	11 Aug 69
3096	"	"	108	0001	14 Jun 69	2201	11 Aug 69
3102	39°10.0'	70°02.4'	532	1719	11 Aug 69	1319	12 Oct 69
3103	"	"	1044	1729	11 Aug 69	0129	7 Dec 69
3104	"	"	2066	1741	11 Aug 69	1141	8 Dec 69
3143	34°02.7'	70°02.0'	14	1653	13 Aug 69	1653	8 Oct 69

RECORD	LAT. N	LONG. W	DEPTH m.	START TIME GMT	START DATE	STOP TIME GMT	STOP DATE
3176	39°12.0'	70°02.8'	207	1623	6 Oct 69	1623	3 Dec 69
3233	33°58.5'	69°58.5'	515	2052	8 Jan 70	1852	9 Mar 70
3234	"	"	1017	2115	8 Jan 70	1915	9 Mar 70
3236	"	"	2020	2102	8 Jan 70	2102	9 Mar 70
3237	"	"	4205	2123	8 Jan 70	2123	9 Mar 70
3261	37°37.0'	70°00.0'	3990	1845	28 Feb 70	1245	8 Jul 70
3291	31°00.0'	70°29.0'	4209	0145	4 Mar 70	0743	5 Jul 70
3342	33°58.0'	69°56.0'	14	2223	14 May 70	0423	6 Jul 70
3344	"	"	1017	2208	14 May 70	0608	26 Jun 70
3345	"	"	2019	2208	14 May 70	0608	6 Jul 70
3351	32°08.0'	64°07.5'	1312	0838	17 May 70	0638	2 Jul 70
3354	"	"	2346	0823	17 May 70	0823	2 Jul 70
3385	39°34.5'	69°55.5'	52	2016	27 Jun 70	1416	17 Aug 70
3386	"	"	72	2016	27 Jun 70	1416	17 Aug 70
3387	"	"	2167	2016	27 Jun 70	1416	17 Aug 70
3395	39°07.6'	70°02.3'	52	0731	28 Jun 70	0331	18 Aug 70
3396	"	"	72	0731	28 Jun 70	0331	18 Aug 70
3397	"	"	2545	0731	28 Jun 70	0331	18 Aug 70
3404	39°07.5'	70°35.2'	52	1716	28 Jun 70	0316	18 Aug 70
3406	"	"	72	1716	28 Jun 70	0316	18 Aug 70
3407	"	"	2620	1716	28 Jun 70	0316	18 Aug 70
3432	35°58.0'	70°33.0'	2263	1630	13 Aug 70	1030	30 Sep 70
3434	"	"	4115	1630	13 Aug 70	1430	8 Oct 70
3451	39°28.5'	70°58.6'	1504	0100	19 Aug 70	1700	6 Oct 70
3461	39°35.5'	70°58.0'	2163	0430	19 Aug 70	1230	11 Dec 70
3481	39°50.2'	70°57.0'	975	1915	19 Aug 70	1315	6 Oct 70
3491	39°50.6'	70°56.2'	846	2030	19 Aug 70	1230	6 Oct 70
3492	"	"	933	2030	19 Aug 70	1230	6 Oct 70
3493	"	"	941	2030	19 Aug 70	1230	6 Oct 70
3501	39°49.6'	70°56.0'	888	2146	19 Aug 70	1346	12 Oct 70
3502	"	"	990	2146	19 Aug 70	2346	16 Nov 70

usually separated by fifteen minutes. Obviously bad values were replaced by interpolated values. The burst averages were further averaged to an east and north velocity component for every two hours.

The working data was Fourier coefficients for the records in Table 2, which were read from a tape of Dr. William Schmitz at the Woods Hole Oceanographic Institution. No other smoothing or filtering of the data had been done beyond the two hour averaging. On the tapes were cosine and sine coefficients, a_n and b_n, at each computed frequency for both east (u) and north (v) velocities. These determined an amplitude, $(a_n^2 + b_n^2)^{1/2}$, and phase, $\arctan(a_n/b_n)$, at each frequency. Thus for each frequency ω_n there are east and north velocity components which can be written as

$$u = u_n \cos(\omega_n + \alpha) \quad \text{and}$$
$$v = v_n \cos(\omega_n + \beta) \ ,$$

which add vectorially to give a total velocity. This total velocity sweeps out an ellipse every $2\pi/\omega_n$ hours.

Each Fourier coefficient tells how much cosine wave at what phase would have to be added to simulate the record. If there is a strong periodicity in the record, this will show up as a peak at that frequency in a graph of the Fourier coefficient amplitudes versus frequency. It was hoped that the Fourier coefficients for the data

used here would show recognizable peaks at some of the main tidal forcing frequencies. Plots of Fourier coefficient amplitude versus frequency around diurnal and semidiurnal frequencies over a width of .0110 cycles per hour were inspected for presence of internal tides. To be considered a peak, a Fourier coefficient amplitude usually had to be the largest value on the graph except for a peak at one of the other tidal periods. The decision was subjective. Sometimes there was a problem deciding at which frequency to look for the peak. The record length determines the frequencies at which the Fourier coefficients are computed so that the M_2 coefficient will not in general be exactly at a period of 12.42 hours. To have some base for comparison, Fourier transforms of equilibrium tides were computed. By finding the Fourier coefficients of the equilibrium tide for a record, one at least sees how a record of that length picks out tidal periodicities. For instance Figure 2 shows the Fourier coefficient amplitudes for record 1892 and the equilibrium tide associated with 1892. Looking at the equilibrium coefficients, one sees that if record 1892 has strong periodic components at the M_2 and S_2 frequencies, they will show up as peaks at 1/12.47 and 1/12.04 cycles/hour. The east (u) component of 1892 shows definite peaks at these frequencies. For this component of the record the M_2 and S_2

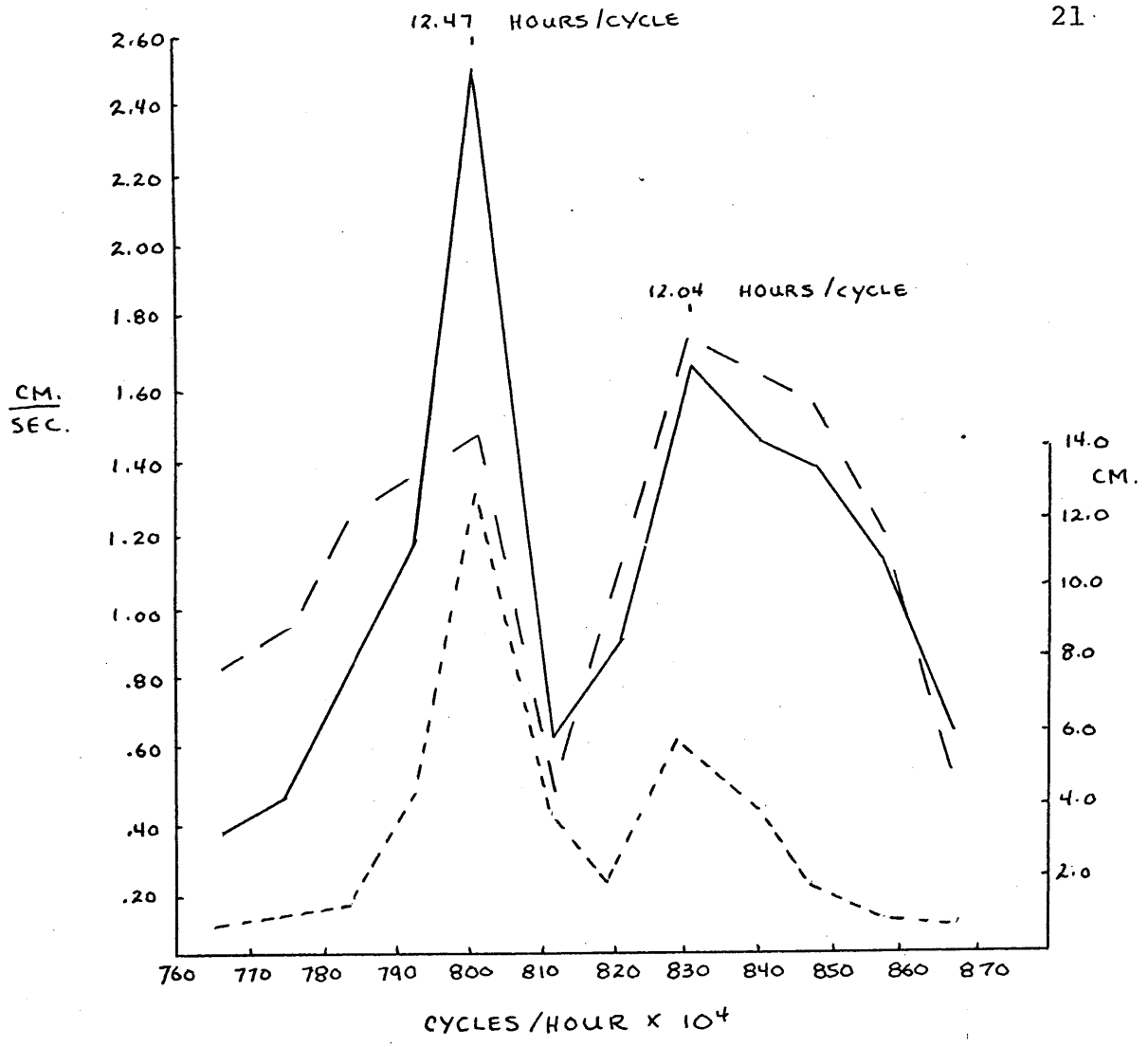

FIGURE 2

FOURIER COEFFICIENT AMPLITUDES FOR 1892

——— FOR EAST VELOCITY IN CM/SEC.

— — FOR NORTH VELOCITY IN CM/SEC.

------ FOR EQUILIBRIUM TIDE IN CM.

peaks are even in something of the same proportion as in the equilibrium tide. The M_2 and S_2 internal tides in the north (v) velocity component are not as clear, but there still seem to be peaks at both periods. Only the M_2 peak showed up in a good number of the records. The number of records having peaks at the main tidal frequencies is shown below. Again, the choice of what to call a peak was a subjective, eyesight determination. The total number of records is 58.

	M_2	S_2+K_2	O_1	K_1+P_1
u	36	10	9	12
v	22	8	7	11

Since the M_2 component is by far the most frequent and usually the dominant of the internal tides, all the analysis that follows is done on the M_2 internal tide so that this is more exactly a study of the M_2 internal tides in these 58 records.

Noise in the records introduces errors and bias into the Fourier coefficients. The observed Fourier coefficient amplitude, say E, is partly tidal, H, and partly noise, n. An unbiased estimate of H is $(E^2 - n^2)^{1/2}$, and one standard deviation error bars are approximately $\pm\ n/\sqrt{2}$ (WUNSCH, 1967). Only crude estimates of n can be made. Looking at Figure 2, one might figure that by .0760 and .0870 cycles/hour the signal has dropped off

to mostly noise. Estimating the noise, n, for 1892-u to be the average of the first two and the last two values in the range .0760 to .0870 cycles/hour gives a value of n = .60 cm/sec. Since the raw Fourier coefficient amplitude for 1892-u is 2.48 cm/sec, the unbiased estimate with n = .60 cm/sec is $H = (2.48^2 - .60^2)^{1/2} =$ 2.41 cm/sec, and one standard deviation error bars for H are approximately $\pm$ .42 cm/sec. The value for n is of course only a rough estimate. Unbiased estimates for the amplitudes and error bars were computed similarly for the other records.

The phase estimates from the Fourier transforms are unbiased but are still subject to errors introduced by the noise. The phase error bars are a function of the signal to noise ratio, H/n. Using the results of Middleton (1948), Wunsch has estimated the integral of the probability density function for the phase of a narrow band, random process in the presence of noise for H/n = 1.0, 1.5, 2.0, 2.5, 3.0, 3.5, and 4.0. A rough plot of 95% confidence limits versus H/n was drawn using Wunsch's values. The phase error bars were estimated from this rough graph. The graph ended at H/n = 4.0, but the slope of the curve was small by H/n = 4.0, so records with $H/n > 4.0$ were given the value at H/n = 4.0, about 20°, as an upper bound value.

The Fourier coefficients for u (east) and v (north) velocity observed above the noise level are shown in Table 3. The error bars on the unbiased amplitudes approximate one standard deviation, and the phase error bars are approximate 95% confidence limits.

The Fourier coefficients indicate that the M_2 internal tide is quite variable. As a case in point, Figures 3 and 4 show the Fourier coefficient amplitudes for frequencies between .0760 and .0870 cycles per hour for both u and v components of all meters on moorings 189 and 212. Mooring 189 was at 39°20'N, 69°57'W in late fall 1965, and mooring 212 was at 39°20'N, 69°52'W in late fall 1966. In both cases the shallowest meter shows highest M_2 amplitudes, but 212 shows no sign of the S_2 internal tide seen in 189. The record for near 1000 meters on 189 shows definite M_2 and S_2 peaks. The Fourier coefficient amplitudes for 1895 are below the M_2 and S_2 peaks for 1894 and show no strong M_2 or S_2 peaks of their own. For mooring 212 on the other hand, the meter at 2000 meters has M_2 peaks above the Fourier coefficient amplitudes for the meter near 1000 meters. The east component of record 2124 does show a definite M_2 peak, but this is nearly half the height of the peak for 1894-u. The internal tide shows very different characteristics at these two moorings.

TABLE 3

FOURIER COEFFICIENTS

REC	DEPTH m.	LAT °N	EAST(u) RAW AMP cm/sec	EAST(u) UNBIASED AMP cm/sec	EAST(u) PHASE °	NORTH(v) RAW AMP cm/sec	NORTH(v) UNBIASED AMP cm/sec	NORTH(v) PHASE °
1892	99	39°20'	2.48	2.41±.42	306±20	1.41	1.16±.57	205±68
1894	1001	"	1.01	.98±.15	306±20	.50	.47±.12	171±27
1895	2002	"	---	---	---	---	---	---
1932	492	39°19'	.56	.51±.16	325±34	---	---	---
1933	994	"	.81	.76±.19	271±27	---	---	---
2121	50	39°20'	2.13	2.06±.35	108±20	---	---	---
2124	950	"	.52	.51±.08	184±20	---	---	---
2125	1950	"	.97	.95±.13	188±20	.35	.30±.13	143±50
2203	106	39°18'	2.43	2.37±.40	202±20	1.82	1.78±.25	112±20
2204	511	"	.96	.86±.30	228±43	---	---	---
2205	1013	"	.70	.65±.17	221±28	---	---	---
2651	2578	39°11'	.37	.33±.11	309±40	---	---	---
2681	2671	39°10'	---	---	---	---	---	---
2743	54	39°10'	---	---	----	---	---	---
2843	54	39°10'	---	---	---	---	---	---
2871	2580	39°11'	1.10	1.07±.16	20±20	.69	.60±.24	319±46
2983	14	39°09'	3.60	3.50±.58	345±20	2.89	2.80±.52	271±21
3021	2586	39°06'	.65	.63±.11	38±20	---	---	---
3041	4287	36°23'	.58	.54±.16	87±32	.58	.56±.11	263±22
3051	4227	36°43'	.50	.47±.13	103±29	.50	.48±.10	331±22

REC.	DEPTH m.	LAT. °N	EAST(u) RAW AMP. cm/sec	EAST(u) UNBIASED AMP. cm/sec	EAST(u) PHASE °	NORTH(v) RAW AMP. cm/sec	NORTH(v) UNBIASED AMP. cm/sec	NORTH(v) PHASE °
3093	13	39°09'	----	---	---	----	---	---
3095	56	"	1.74	1.67±.36	198±23	----	---	---
3096	108	"	1.62	1.54±.34	141±23	----	---	---
3102	532	39°10''	.70	.67±.15	346±23	----	---	---
3103	1044	"	1.11	1.11±.07	287±20	.33	.32±.07	212±23
3104	2066	"	1.04	1.03±.08	341±20	----	---	---
3143	14	34°03'	1.20	1.07±.39	197±46	1.56	1.38±.51	90±46
3176	207	39°12'	----	---	---	----	---	---
3233	515	33°59'	1.18	1.13±.24	326±23	1.24	1.20±.22	270±20
3234	1017	"	.75	.66±.26	245±50	----	---	---
3236	2020	"	.52	.46±.17	148±46	.96	.91±.23	12±27
3237	4205	"	.46	.46±.05	130±20	.64	.64±.04	18±20
3261	3990	37°37'	----	---	---	----	---	---
3291	4209	31°00'	.42	.42±.03	305±20	----	---	---
3342	14	33°58'	1.46	1.26±.51	66±53	1.42	1.19±.54	344±58
3344	1017	"	----	---	---	.90	.85±.19	148±23
3345	2019	"	----	---	---	----	---	---
3351	1312	32°08'	1.00	.91±.29	185±37	.93	.87±.22	74±27
3354	2346	"	.53	.53±.05	125±20	.60	.59±.07	15±20
3385	52	39°35'	----	---	---	----	---	---
3386	72	"	----	---	---	----	---	---
3387	2167	"	1.32	1.30±.20	47±20	.63	.57±.18	353±37
3395	52	39°08'	----	---	---	1.13	.96±.42	239±58
3396	72	"	----	---	---	1.68	1.58±.40	240±27
3397	2545	"	.84	.80±.15	86±21	----	---	---

			EAST(u)			NORTH(v)		
REC.	DEPTH m.	LAT. °N	RAW AMP. cm/sec	UNBIASED AMP. cm/sec	PHASE °	RAW AMP. cm/sec	UNBIASED AMP. cm/sec	PHASE °
3404	52	39°08'	3.05	2.99±.43	199±20	2.39	2.29±.49	117±23
3406	72	"	2.70	2.64±.40	206±20	2.04	1.94±.45	121±25
3407	2620	"	----	---	---	----	---	---
3432	2263	35°58'	----	---	---	----	---	---
3434	4115	"	----	---	---	----	---	---
3451	1504	39°29'	.70	.69±.07	88±20	.16	.14±.05	306±43
3461	2163	39°36'	----	---	---	----	---	---
3481	975	39°50'	----	---	---	----	---	---
3491	846	39°51'	.85	.83±.14	230±20	----	---	---
3492	933	"	----	---	---	----	---	---
3493	941	"	----	---	---	----	---	---
3501	888	39°50'	1.10	1.08±.15	242±20	----	---	---
3502	990	"	----	---	---	----	---	---

EAST

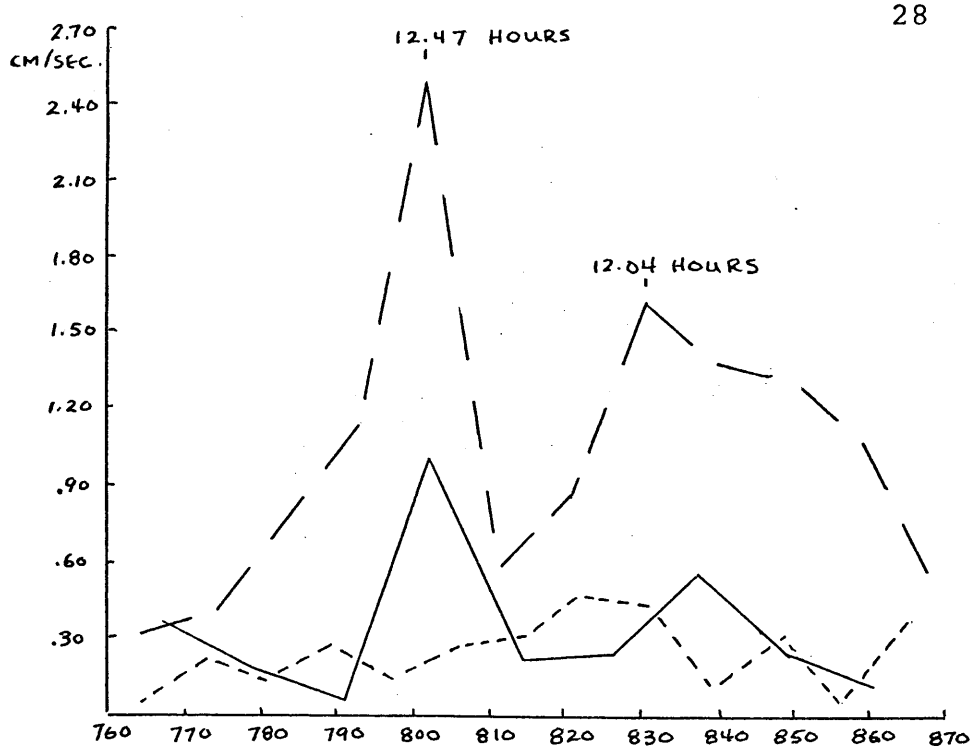

NORTH

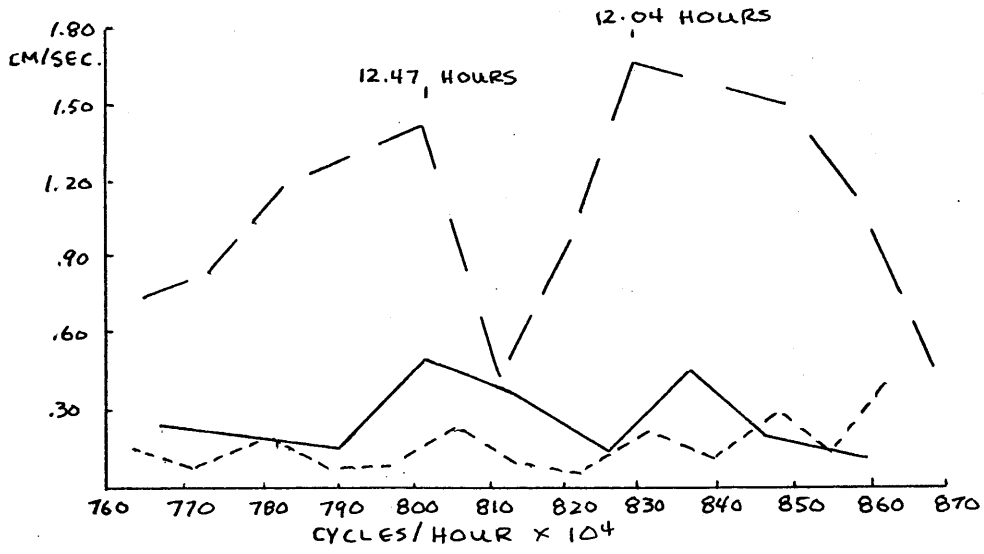

FIGURE 3

FOURIER COEFFICIENT AMPLITUDES FOR MOORING 189

—— —— FOR 1892 AT 99 METERS

———— FOR 1894 AT 1001 METERS

------- FOR 1895 AT 2002 METERS

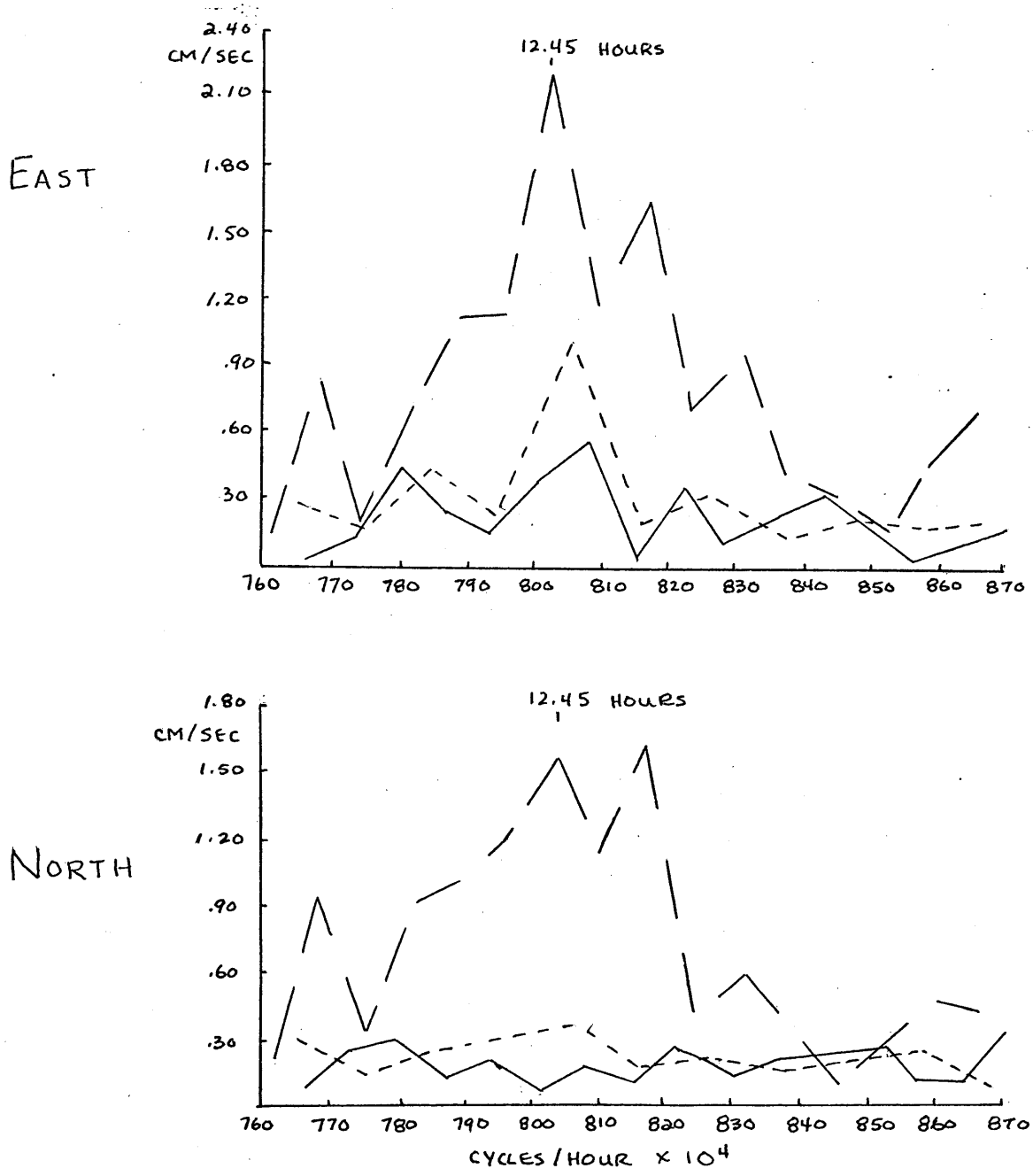

FIGURE 4

FOURIER COEFFICIENT AMPLITUDES FOR MOORING 212

—— —— FOR 2121 AT 50 METERS

———— FOR 2124 AT 950 METERS

- - - - - FOR 2125 AT 1950 METERS

Most of the moorings show a depth dependence more similar to mooring 189 than to 212. For the values in Table 3 only moorings 193, 212, 310, and 339 show instances where for the same component a deeper record has a lower M_2 amplitude than a shallower record on the same mooring. For both moorings 189 and 212 the M_2 peaks in the east velocity are larger than those in the north velocity coefficients. The east M_2 velocities appear to be larger for most Site D records, especially those in deep water, but this does not appear to be so true for the records from south of Site D.

The variation over time of the M_2 internal tide makes looking for latitudinal or longitudinal variations in the internal tide difficult. If the internal tide at Site D is generated at the continental shelf to the north, as Rattray's (1960 and 1969) model would suggest, then the internal tide would be expected to lose energy as it travels south and show larger fluctuations to the north. Attempts to find any such variation in records at about the same depth proved inconclusive, possibly due to large variations in the character of the M_2 internal tide between the times of the records. According to the beam theory, comparing moorings at about the same depth may actually be misleading, since the same beam would appear at different depths on separated moorings.

Since records are in general of different lengths and starting times, the phases from the Fourier transforms are not readily comparable. Inspection of the M_2 phases is better left to the section on admittances, where the phases are normalized with respect to the equilibrium tide.

III. ADMITTANCES

Because the Fourier coefficient amplitudes and phases are affected by the record length and beginning time of the record, a normalization of the Fourier coefficients with respect to the equilibrium tide was computed for each of the unbiased Fourier coefficients in Table 3. First, equilibrium tidal heights at the position and times corresponding to a particular record were computer generated. For instance for record 1892 an equilibrium tidal height was calculated for 39°20.0'N, 69°57.0'W every two hours from 0006 GMT on October 7, 1965, until 1406 November 20, 1965. The equilibrium tide is the surface tide on a rigid, spherical earth in a massless ocean. It represents the instantaneous height of the geopotentials and hence the tidal forcing. A fast Fourier transform was then performed on the computed equilibrium tidal heights. If $\hat{H} = |\hat{H}| e^{i(\omega t + \hat{\theta})}$ is the unbiased Fourier coefficient at M_2 frequency and $\hat{\mathcal{J}} = |\hat{\mathcal{J}}| e^{i(\omega t + \hat{\varphi})}$ is the same for the equilibrium tide, then the admittance is defined as $\frac{\hat{H}}{\hat{\mathcal{J}}} = \frac{|\hat{H}|}{|\hat{\mathcal{J}}|} e^{i(\hat{\theta} - \hat{\varphi})}$.

The M_2 admittance is a normalized observed M_2 component with amplitude $|H|/|\mathcal{J}|$ and phase $\hat{\theta} - \hat{\varphi}$. The admittances

for records with a peak at M_2 frequency are given in Table 4.

Since the approximate lunar equilibrium tide is $0.584(3\cos^2\theta - 1)$ (SCHUREMAN, p.29) where θ is the latitude, the M_2 admittance amplitude for records at nearly the same latitude normalizes for how well the record length picks out a periodicity of M_2 frequency. The number of data points determines at what frequencies the Fourier coefficients are computed, so the same M_2 signal can be found as Fourier coefficients with different amplitudes in the Fourier transforms of different sized records. A record of length such that a coefficient is computed at a frequency of 1/12.42 cycles/hour will show the same M_2 fluctuation as a larger peak than a record which gives transform values at frequencies straddling the M_2 frequency. One would like, however, to have a measure which is nearly the same for the same signal, independent of record length. For records at nearly the same latitude, such as those at Site D, the M_2 admittance amplitude gives such a normalization. A record at 39°N will have an equilibrium tidal amplitude of about 3/4 of that at 34°N, so that comparison of M_2 admittance amplitudes at such different latitudes includes normalizing for the tidal forcing as well as record length. Comparison between records of Fourier coefficient phases

is difficult, since the phases are relative to the starting time of the records and are also affected by the frequencies at which the coefficients are calculated. The admittance phase at least gives the M_2 phase relative to the same equilibrium tide.

Comparing Tables 3 and 4, one sees that the normalization changes some of the relative amplitudes, but the admittance amplitudes show the same general characteristics as the Fourier coefficient amplitudes. In both cases the same moorings are exceptions to the rule that for u and v considered separately, deeper meters on the same mooring have lower amplitudes. The differences in Fourier coefficient amplitudes between records 1894 and 2124 still appear with the normalization. Record 1894 appears to be in phase with 1892. Record 2121 has about the same admittance phase as 1892, but 2124, which is at about the same depth as 1894, appears to be 180° out of phase with 2121. None of these is within the confidence limits of being exactly in or out of phase with the equilibrium tide. The phases for 3404 and 3406 are similar to those for 1892 and 2121, all of which are shallow Site D records. Site D admittance phases show various other values, several of which are with the confidence limits of being in phase with the equilibrium tide.

TABLE 4

ADMITTANCES

REC.	DEPTH m.	LAT. °N	EAST(u) AMP.	EAST(u) PHASE °	NORTH(v) AMP.	NORTH(v) PHASE °
1892	99	39°20'	.185±.03	308±20	.089±.04	207±68
1894	1001	"	.070±.01	316±20	.034±.01	181±27
1895	2002	"	---	---	---	---
1932	492	39°19'	.054±.02	231±34	---	---
1933	994	"	.075±.02	6±27	---	---
2121	50	39°20'	.172±.03	306±20	---	---
2124	950	"	.044±.00	140±20	---	---
2125	1950	"	.062±.01	10±20	.019±.01	325±50
2203	106	39°18'	.169±.03	38±20	.127±.02	308±20
2204	511	"	.068±.02	113±43	---	---
2205	1013	"	.049±.01	92±28	---	---
2651	2578	39°11'	.028±.01	308±40	---	---
2681	2671	39°10'	---	---	---	---
2743	54	39°10'	---	---	---	---
2843	54	39°10'	---	---	---	---
2871	2580	39°11'	.084±.01	211±20	.047±.02	150±46
2983	14	39°09'	.251±.04	352±20	.201±.04	278±21
3021	2586	39°06'	.056±.01	92±20	---	---
3041	4287	36°23'	.039±.01	190±32	.040±.01	315±22
3051	4227	36°43'	.041±.01	220±29	.042±.01	88±22
3093	13	39°09'	---	---	---	---
3095	56	"	.129±.03	28±23	---	---
3096	108	"	.110±.02	254±23	---	---
3102	532	39°10'	.061±.01	357±23	---	---
3103	1044	"	.081±.01	249±20	.023±.01	174±23
3104	2066	"	.095±.01	344±20	---	---
3143	14	34°03'	.077±.03	255±46	.110±.04	148±46

REC.	DEPTH m.	LAT. °N	EAST(u) AMP.	EAST(u) PHASE °	NORTH(v) AMP.	NORTH(v) PHASE °
3176	207	39°12'	---	---	---	---
3233	515	33°59'	.069±.01	239±23	.073±.01	182±20
3234	1017	"	.040±.02	147±50	---	---
3236	2020	"	.028±.01	27±46	.056±.01	251±27
3237	4205	"	.028±.00	358±20	.038±.00	246±20
3261	3990	37°37'	---	---	---	---
3291	4209	31°00'	.028±.00	246±20	---	---
3342	14	33°58'	.076±.03	93±53	.072±.03	12±58
3344	1017	"	---	---	.050±.01	209±23
3345	2019	"	---	---	---	---
3351	1312	32°08'	.055±.02	353±37	.052±.01	243±27
3354	2346	"	.031±.00	273±20	.034±.01	163±20
3385	52	39°35'	---	---	---	---
3386	72	"	---	---	---	---
3387	2167	"	.105±.02	109±20	.046±.02	56±37
3395	52	39°08'	---	---	.075±.03	335±58
3396	72	"	---	---	.123±.03	337±27
3397	2545	"	.062±.01	183±21	---	---
3404	52	39°08'	.232±.03	303±20	.178±.04	221±23
3406	72	"	.205±.03	310±20	.151±.03	226±25
3407	2620	"	---	---	---	---
3432	2263	35°58'	---	---	---	---
3434	4115	"	---	---	---	---
3451	1504	39°29'	.055±.01	205±20	.011±.00	64±43
3461	2163	39°36'	---	---	---	---
3481	975	39°50'	---	---	---	---
3491	846	39°51'	.072±.01	129±20	---	---
3492	933	"	---	---	---	---
3493	941	"	---	---	---	---
3501	881	39°50'	.084±.01	180±20	---	---
3502	990	"	---	---	---	---

IV. TIDAL ELLIPSES

The Fourier coefficients at each frequency determine an east (u) and north (v) velocity which can be represented as

$$u = A_1\cos(\omega t) + B_1\sin(\omega t) \quad \text{and}$$

$$v = A_2\cos(\omega t) + B_2\sin(\omega t).$$

The total velocity, $\underline{u}$, sweeps out an ellipse every $2\pi/\omega$ hours. Each ellipse can be described completely by five parameters - velocity direction at the initial time, velocity amplitudes at the major and minor axes, direction of the major axis counterclockwise from east, and rotational direction (clockwise or counterclockwise). At the suggestion of Dr. William Schmitz, the parameters of the ellipse for each frequency were printed out when the Fourier coefficients were read from the tape.

The method for finding the parameters of the ellipses followed essentially that found in Doodson and Warburg (1941) except for inserting a missing two. The squared magnitude of the total velocity can be written as

$$|\underline{u}|^2 =$$

$$[A_1\cos(\omega t) + B_1\sin(\omega t)]^2 + [A_2\cos(\omega t) + B_2\sin(\omega t)]^2 =$$

$$C\cos^2(\omega t) + D\sin^2(\omega t) + 2E\sin(\omega t)\cos(\omega t),$$

where $C = A_1^2 + A_2^2$,

$D = B_1^2 + B_2^2$,

and $E = A_1B_1 + A_2B_2$.

With $F = (C - D)/2$

and $G = (C + D)/2$,

$$|\underline{u}|^2 = F \cos(2\omega t) + E \sin(2\omega t) + G.$$

This can be written again as

$$|\underline{u}|^2 = G + H \cos[2(\omega t - a)],$$

where $F = H \cos(2a)$

and $E = H \sin(2a)$,

so that $H^2 = E^2 + F^2$.

In Doodson and Warburg (1941) there is an "a" instead of "2a" in the expressions for E and F. Gerges (1966) also has this mistake. If H is taken as $+(E^2 + F^2)^{1/2}$, then since $|\underline{u}|^2 = G + H \cos[2(\omega t - a)]$, $|\underline{u}|^2$ is at its maximum when $\omega t = a$ and at a minimum when $\omega t = a + 90°$. The angle 2a is the unique angle in $[0, 2\pi)$ whose cosine is F/H and whose sine is E/H. The orientation of the major axis is determined by the values of u and v at $\omega t = a$. The sense of rotation, clockwise or counterclockwise, can be obtained from the position of the velocity vector at a and a + 90°, since the vector must go through an angle of less than 180° when ωt goes from a to a + 90°.

The basic ellipse parameters (except for starting velocity direction which is not important here) plus axis ratios for the more reliable ellipses are given in Table 5, and the major and minor axes for these ellipses are shown in Figures 5- 10. The ellipses shown are those for records with a peak in total power, $u^2 + v^2$, at M_2 frequency. This criterion was chosen arbitraily, and the decision is subjective. Of the ellipses in Table 5 only 2124 and 3041 go counterclockwise. It is possible to calculate a clockwise and counterclockwise component for each ellipse (GONELLA, 1971) as Perkins (1970) did to show the clockwise character of his inertial oscillations; however, the ellipticity and sense of rotation essentially give that information. A nearly circular, clockwise ellipse will be mostly clockwise, while a highly elliptical, clockwise ellipse will have just a slightly greater clockwise than counterclockwise component. This statement holds with clockwise replaced with counterclockwise and vise versa. The exact expression for the relation between the ratic of the clockwise to the counterclockwise amplitude and the ellipticity (ratio of minor to major axis) and sense of rotation is given in Appendix I. For here it is sufficient to note that although 2124 and 3041 are counterclockwise, they are highly elliptical and hence just barely more counterclockwise than clockwise.

TABLE 5 - M_2 TIDAL ELLIPSE PARAMETERS

REC.	DEPTH m.	LAT. °N	Vel. at MAJOR AXIS AMP. cm/sec	DIR. (**)	Vel. at MINOR AXIS cm/sec	RATIO of AMPS.
1892	99	39°20'	2.50	171°	1.37	.55
1894	1001	"	1.08	158	.33	.31
1895	2002	"	----	---	----	---
1932	492	39°19'	----	---	----	---
1933	994	"	----	---	----	---
2121	50	39°20'	2.14	353	1.55	.72
2124*	950	"	.54	197	.01	.02
2125	1950	"	1.00	195	.24	.24
2203	106	39°18'	2.43	180	1.82	.75
2204	511	"	1.07	207	.23	.21
2205	1013	"	.77	203	.14	.18
2651	2578	39°11'	----	---	----	---
2681	2671	39°10'	----	---	----	---
2743	54	39°10'	----	---	----	---
2843	54	39°10'	----	---	----	---
2871	2580	39°11'	1.17	22	.57	.49
2983	14	39°09'	3.78	205	2.64	.70
3021	2586	39°06'	.67	343	.27	.40
3041*	4287	36°23'	.82	314	.03	.04
3051	4227	36°43'	.65	314	.29	.45
3093	13	39°09'	----	---	----	---
3095	56	"	1.90	32	1.22	.64
3096	108	"	1.83	40	1.26	.69
3102	532	39°10'	.71	191	.22	.31
3103	1044	"	1.11	184	.32	.29
3104	2066	"	1.05	189	.29	.28
3143	14	34°03'	1.64	114	1.08	.66

(*) Counterclockwise rotating ellipses.

(**) In degrees counterclockwise from east.

REC.	DEPTH m.	LAT. °N	Vel. at MAJOR AXIS AMP. cm/sec	DIR. (**)	Vel. at MINOR AXIS cm/sec	RATIO of AMPS.
3176	207	39°12'	----	---	----	---
3233	515	33°59'	1.51	227	.81	.54
3234	1017	"	.79	160	.26	.33
3236	2020	"	1.04	113	.33	.32
3237	4205	"	.68	114	.40	.59
3261	3990	37°37'	----	---	----	---
3291	4209	31°00'	.46	157	.00	.00
3342	14	33°58'	1.55	39	1.33	.86
3344	1017	"	----	---	----	---
3345	2019	"	----	---	----	---
3351	1312	32°08'	1.12	140	.78	.70
3354	2346	"	.66	306	.45	.68
3385	52	39°35'	----	---	----	---
3386	72	"	----	---	----	---
3387	2167	"	1.38	18	.49	.36
3395	52	39°08'	1.14	281	.87	.76
3396	72	"	1.70	289	1.50	.88
3397	2545	"	----	---	----	---
3404	52	39°08'	3.09	194	2.34	.76
3406	72	"	2.71	188	2.02	.75
3407	2620	"	----	---	----	---
3432	2263	35°58'	----	---	----	---
3434	4115	"	----	---	----	---
3451	1504	39°29'	.71	350	.10	.14
3461	2163	39°36'	----	---	----	---
3481	975	39°50'	----	---	----	---
3491	846	39°51'	.85	174	.42	.49
3492	933	"	----	---	----	---
3493	941	"	----	---	----	---
3501	881	39°50'	1.12	165	.74	.66
3502	990	"	----	---	----	---

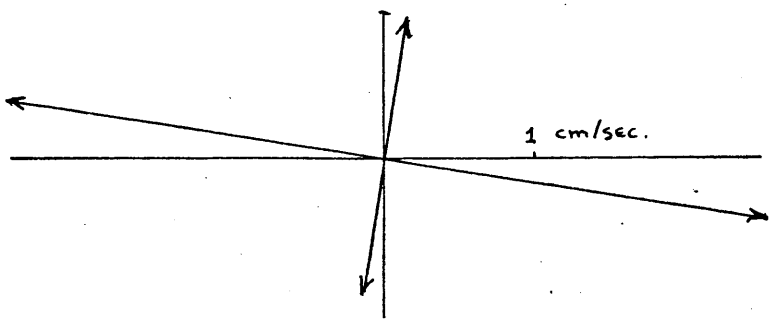

1892 - 99 M.

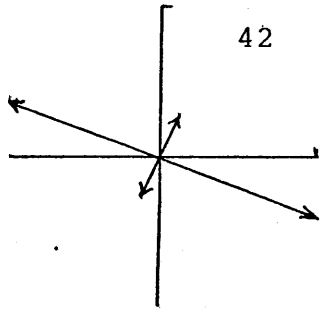

1894 - 1001 M.

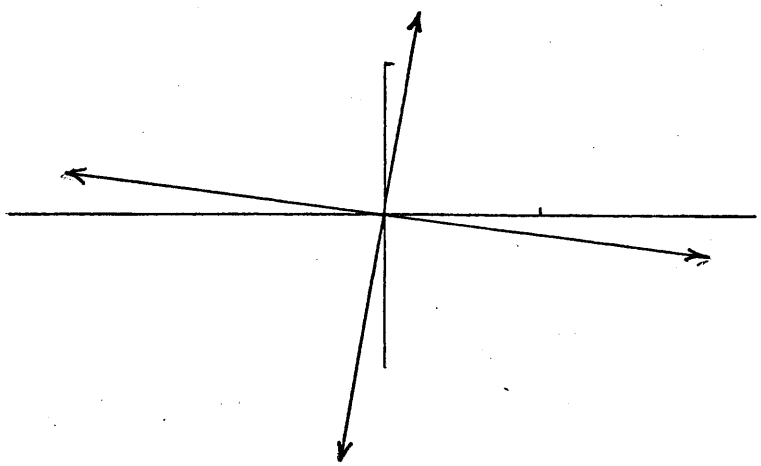

2121 - 50 M.

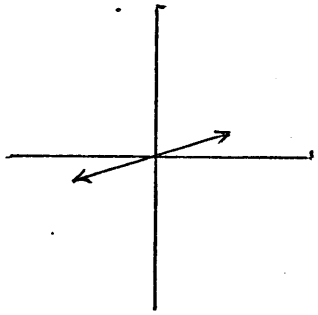

2124 - 950 M.

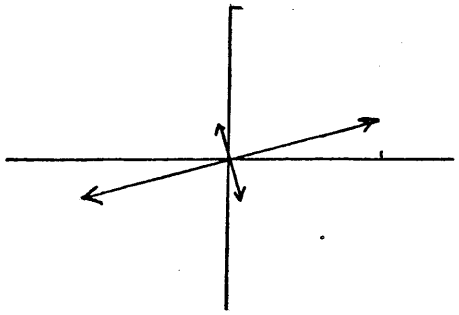

2125 - 1950 M.

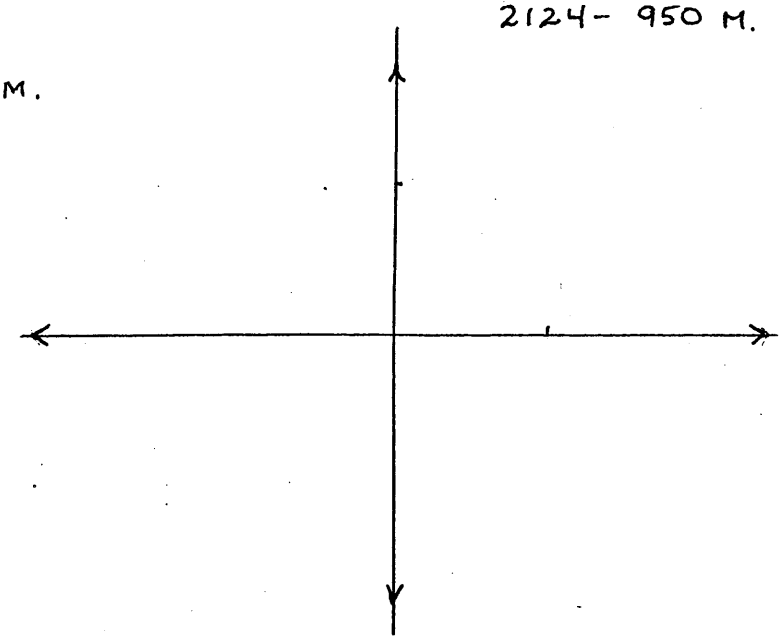

2203 - 106 M.

N

FIGURE 5

TIDAL ELLIPSES AT SITE D

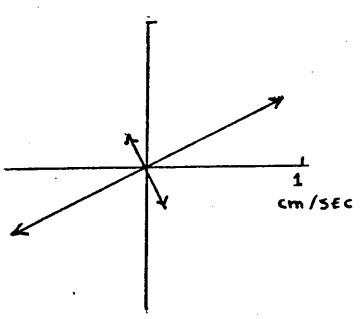

2204 - 511 M.

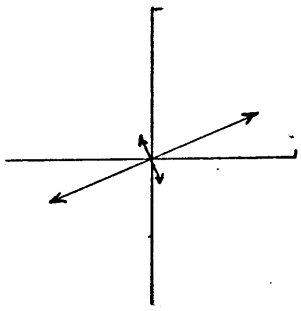

2205 - 1013 M.

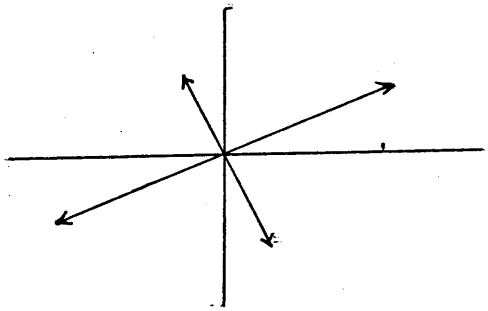

2871 - 2580 M.

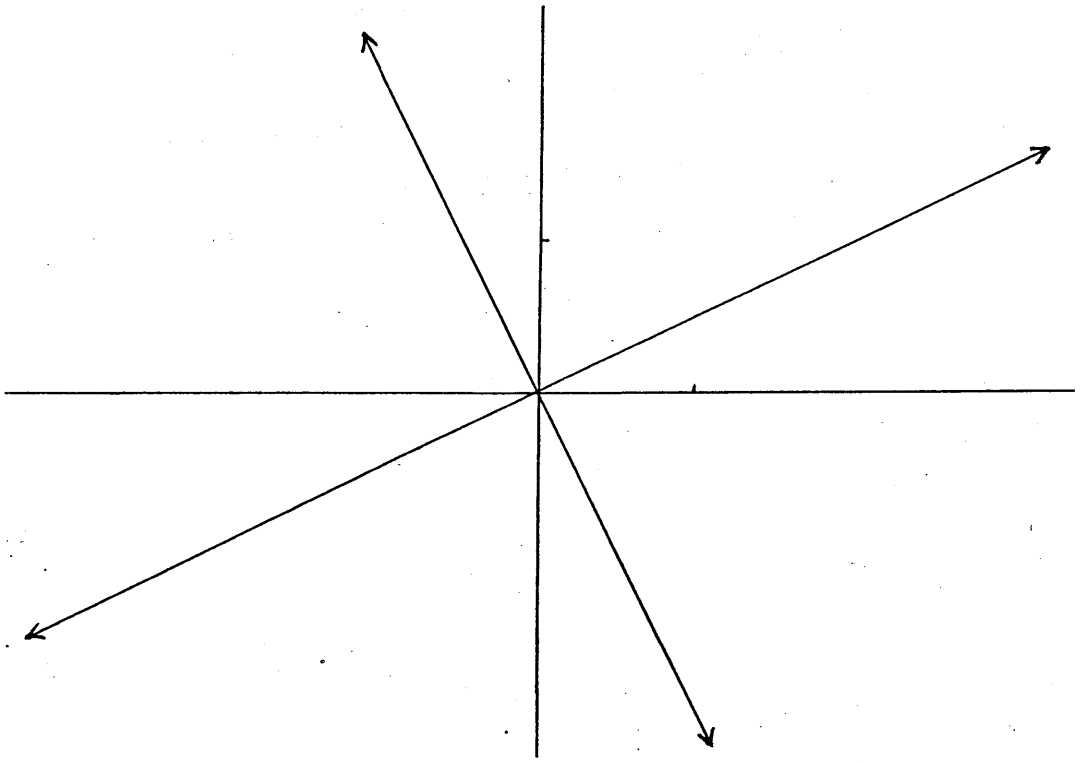

2983 - 14 M.

N

FIGURE 6
TIDAL ELLIPSES AT SITE D

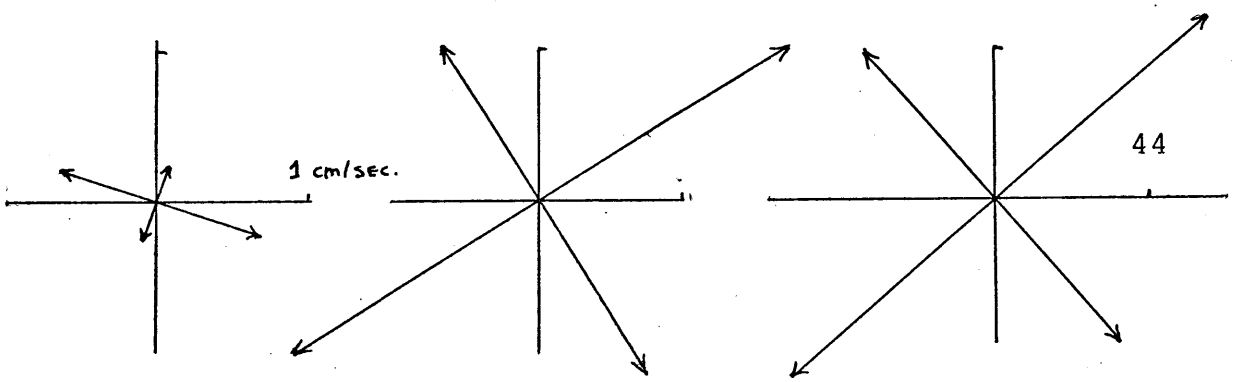

3021 - 2586 M. 3095 - 56 M. 3096 - 108 M.

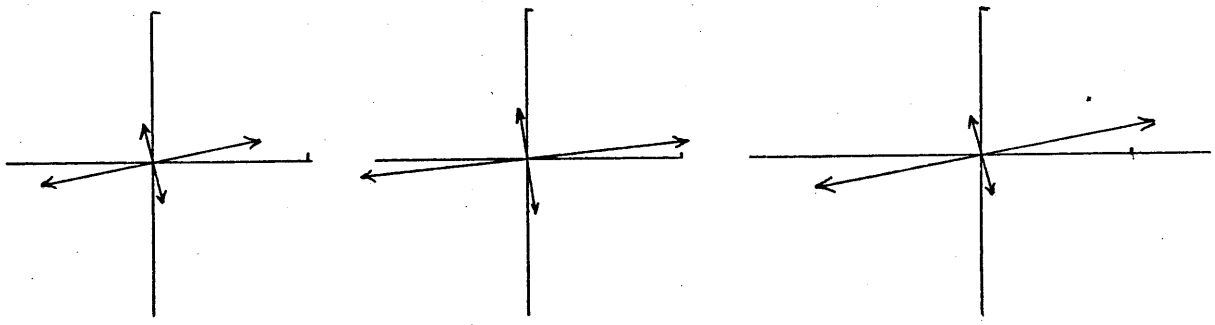

3102 - 532 M. 3103 - 1644 M. 3104 - 2066 M.

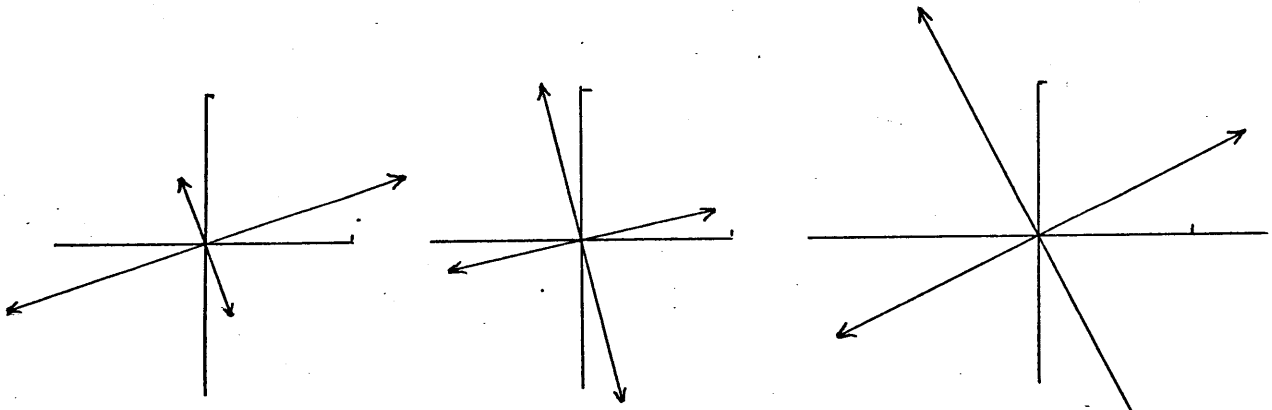

3387 - 2167 M. 3395 - 52 M. 3397 - 72 M.

N

FIGURE 7
TIDAL ELLIPSES AT SITE D

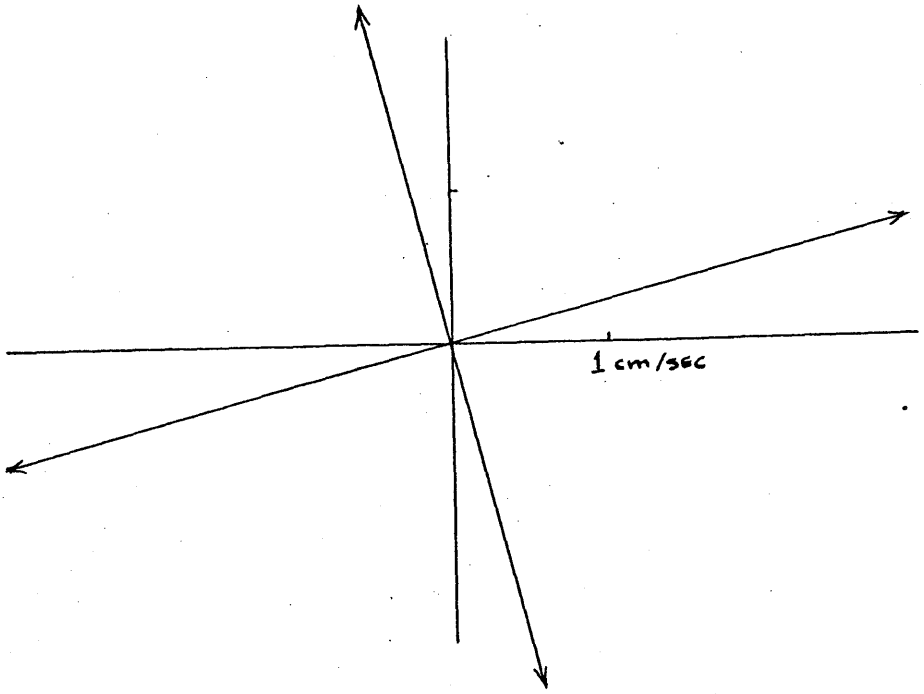

3404 - 52 M.

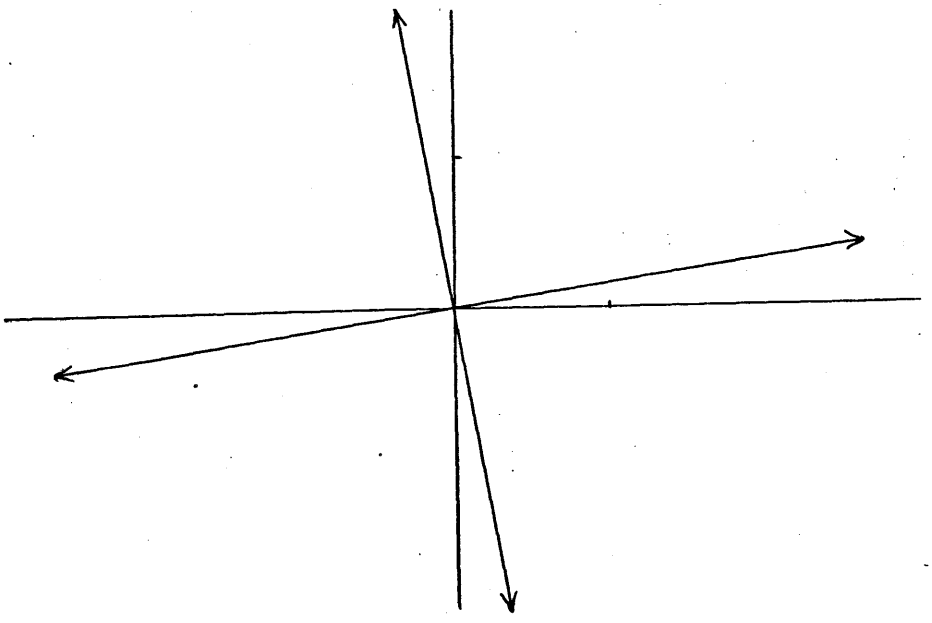

3406 - 72 M.

N

FIGURE 8
TIDAL ELLIPSES AT SITE D

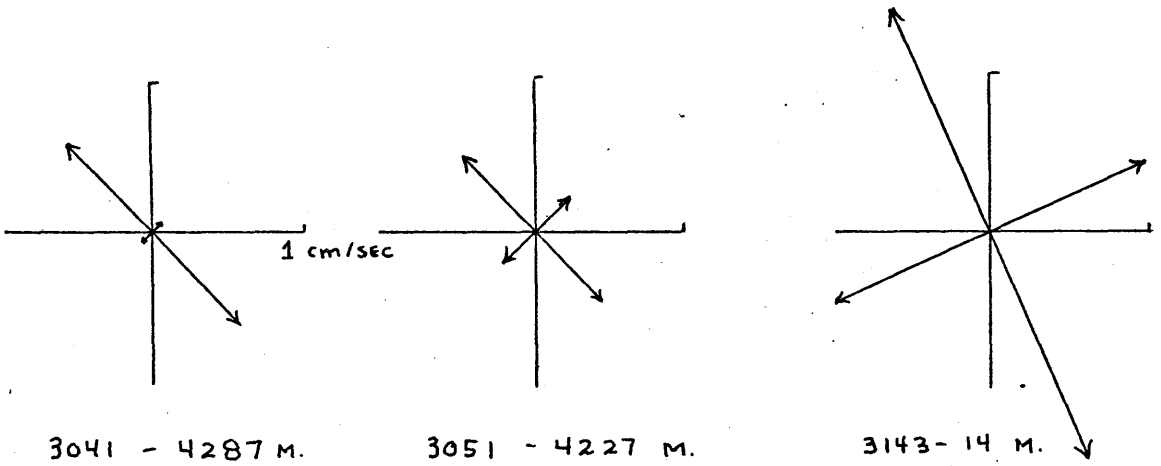

3041 - 4287 M. 3051 - 4227 M. 3143 - 14 M.

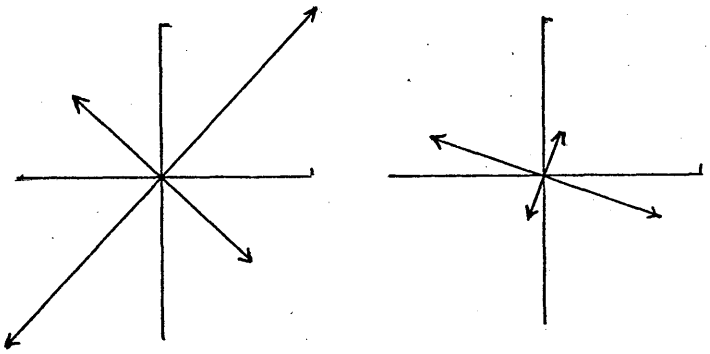

3233 - 515 M. 3234 - 1017 M.

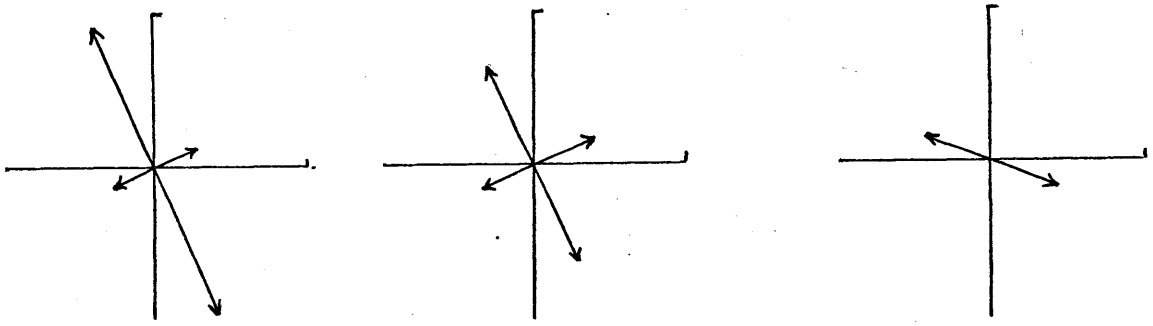

3236 - 2020 M. 3237 - 4205 M. 3291 - 4209 M.

N

FIGURE 9

TIDAL ELLIPSES NOT AT SITE D

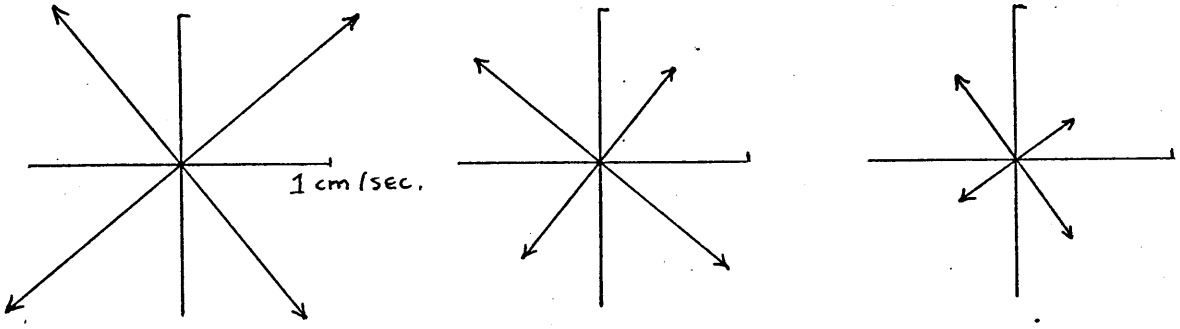

3342 - 14 M.

3351 - 1312 M.

3354 - 2346 M.

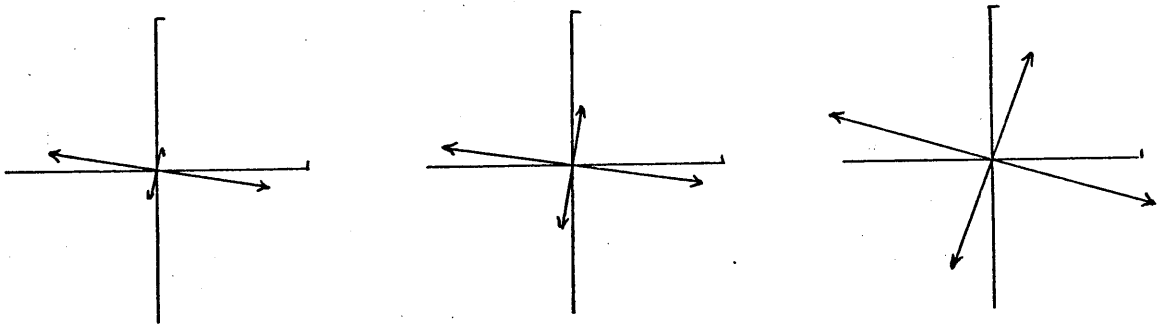

3451 - 1504 M.

3491 - 846 M.

3501 - 888 M.

N

FIGURE 10
TIDAL ELLIPSES NOT AT SITE D

Larger ellipses are found in the shallower water, indicating again the decrease of M_2 fluctuations with increasing depth. The variation of the M_2 internal tide between record 1894 and record 2124 seen before in the Fourier coefficients shows up in the variation of tidal ellipse shapes and amplitudes. Below 200 meters the tidal ellipses at Site D appear to change shape. There the upper layer ellipses appear more circular than those of the deeper water, which tend to be drawn out east-west. The ellipses south of Site D do not tend to show this east-west elongation.

If the internal tide at Site D could be modeled by a single plane wave, this would show up in the shape of the tidal ellipses. If the positive x-direction is taken as east with north the positive y-direction, then periodic u and v must satisfy

$$-i\omega u - fv = -\partial P/\partial x \quad \text{and}$$

$$-i\omega v + fu = -\partial P/\partial y \ .$$

Here f is the inertial frequency, ω is the wave's frequency, and P is the reduced pressure. For Site D internal M_2 tides $f \cong 1/19$ cycles/hour and $\omega = 1/12.42$ cycles/hour. For a plane wave propogating south with wavefronts east-west, $\partial P/\partial x = 0$ so that

$$\frac{u}{v} = \frac{-f}{i\omega} \ .$$

This relation says that u and v are out of phase and in the ratio $-f/\omega$. If starting position is not considered, then to within a constant multiplier, u and v in this case can be represented as

$$u = f \cos(\omega t) \quad \text{and}$$

$$v = -\omega \sin(\omega t) \ .$$

Since $f/\omega \cong 12.42/19$ at Site D, this would be a clockwise ellipse with major axis north-south and ratio of minor to major axis of about .65 . More generally, if the internal tide is considered a plane wave with parallel wavefronts at an angle α so that the partial derivative of the reduced pressure in the direction α is zero, then the horizontal velocity will be a clockwise ellipse with major axis tilted at the angle $\alpha + 90°$ and axis ratio of $f/\omega = .65$. This is shown in Appendix II.

The Rattray model of generation of internal tides at continental shelf edges might suggest trying to model the internal tides at Site D as a plane wave coming from the north. This would show up as north-south elongated ellipses, but the ellipses at Site D tend to have their major axes more east-west than north-south, especially for deeper records. The deep water ellipses at Site D are not consistent with a plane wave coming from any direction, since the ratio of minor to major axes tends to be much smaller than f/ω. Ratios closer to f/ω are found

above 200 meters at Site D and to the south of Site D, but no definite prefered direction can be seen.

V. POWER DENSITIES

For many of the records with no legitimate peak at the M_2 frequency there was still an obvious sign of activity around M_2. Sometimes the peak would be slightly shifted and other times the tidal power would appear to have been smeared over several frequencies. If a record showed a definite sign of a rise in power at around the M_2 frequency, then a power density was calculated. The band width was selected to be most nearly .0028 cycles per hour. Bandwidths varied from .0023 to .0031 cycles per hour. For a medium sized record this meant using four transform values to calculate the power density. The power densities were calculated with the raw Fourier coefficient amplitudes. If E_i represents one of the m Fourier coefficient amplitudes in the band and Δf is the frequency difference between neighboring values, then the power density is estimated by

$$\frac{1}{m(\Delta f)} \sum_{i=1}^{m} E_i^2 \quad .$$

The calculated power densities are given in Table 6. Since values neighboring the exact M_2 frequency are included in the calculation, the power density is independent of the record length, unlike the Fourier coefficients. For

TABLE 6

M_2 POWER DENSITIES

REC.	DEPTH m.	LAT. °N	POWER DENSITY u $\left(\frac{cm}{sec}\right)^2/\frac{cy}{hr}$	v $\left(\frac{cm}{sec}\right)^2/\frac{cy}{hr}$
1892	99	39°20'	2785	1371
1894	1001	"	469	156
1895	2002	"	----	----
1932	492	39°19'	304	144
1933	994	"	368	----
2121	50	39°20'	3385	2714
2124	950	"	200	----
2125	1950	"	322	77
2203	106	39°18'	3871	2200
2204	511	"	542	----
2205	1013	"	325	103
2651	2578	39°11'	133	83
2681	2671	39°10'	----	----
2743	54	39°10'	3093	2453
2843	54	39°10'	----	----
2871	2580	39°11'	613	306
2983	14	39°09'	12542	8242
3021	2586	39°06'	311	162
3041	4287	36°23'	251	192
3051	4227	36°43'	207	162
3093	13	39°09'	33393	24965
3095	56	"	1700	2385
3096	108	"	1957	2457
3102	532	39°10'	311	----
3103	1044	"	571	100
3104	2066	"	514	157
3143	14	34°03'	966	1350

REC.	DEPTH m.	LAT. °N	POWER DENSITY u $(\frac{cm}{sec})^2/\frac{cy}{hr}$	v
3176	207	39°12'	2000	1517
3233	515	33°59'	685	714
3234	1017	"	328	----
3236	2020	"	242	414
3237	4205	"	142	257
3261	3990	37°37'	153	184
3291	4209	31°00'	162	74
3342	14	33°58'	1900	1616
3344	1017	"	400	524
3345	2019	"	----	433
3351	1312	32°08'	666	577
3354	2346	"	133	148
3385	52	39°35'	----	1407
3386	72	"	943	991
3387	2167	"	831	288
3395	52	39°08'	----	1311
3396	72	"	2335	2481
3397	2545	"	607	288
3404	52	39°08'	4335	2831
3406	72	"	3359	1919
3407	2620	"	----	----
3432	2263	35°58'	123	153
3434	4115	"	----	----
3451	1504	39°29'	184	15
3461	2163	39°36'	----	----
3481	975	39°50'	----	----
3491	846	39°51'	353	----
3492	933	"	----	----
3493	941	"	----	----
3501	888	39°50'	554	----
3502	990	"	----	----

the records used here the power density also has the advantage that more records have reliable M_2 power densities than M_2 Fourier coefficients. The power density, though, has less information than Fourier transform values, since the power density has no phase information.

The decrease in amplitude of M_2 fluctuations with increasing depth seen in earlier sections shows up again in the power densities. Generally, deeper meters on the same mooring have lower M_2 power densities. The four moorings which showed exceptions to this rule in the Fourier coefficients and admittances, 193, 212, 310, and 339, are also exceptional in the power densities. The only other mooring for which M_2 power density increases at some lower depth is 309. Meters on different moorings tend to have lower M_2 power densities at greater depths, but the tendency is far from universal. Figures 11 and 12 show log-log plots of the power densities in Table 6 versus depth for east and north velocity components. (Actually, the north power density for 3451 is clear off the graph and is not shown.) Even a log-log plot, which tends to suppress apparent variation, shows considerable variation in the values near any given depth. M_2 power densities for records from below 500 meters are consistently considerably lower, though, than those for the surface layer.

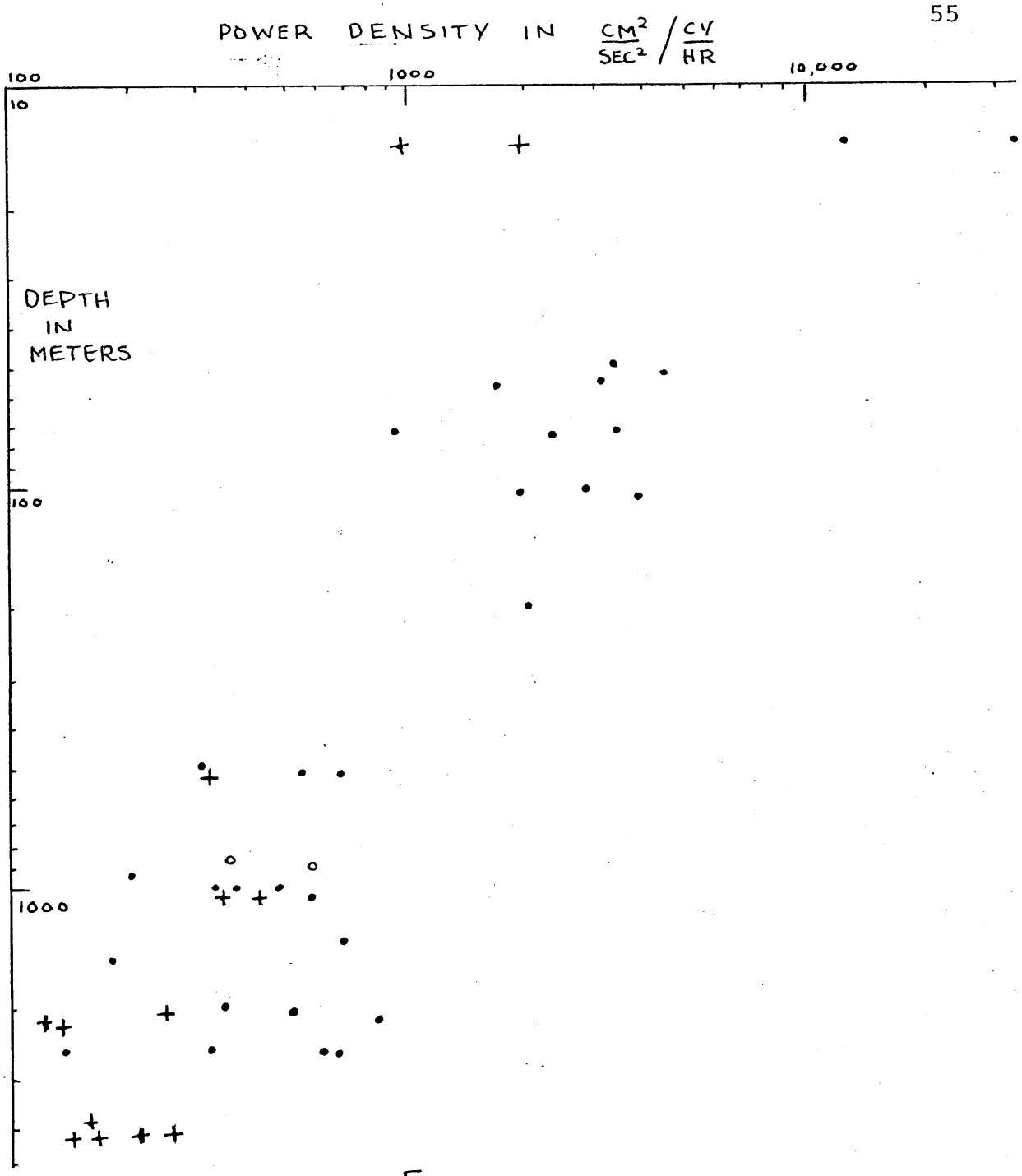

FIGURE 11

M_2 EAST POWER DENSITIES

• FOR SITE D

+ FOR SOUTH OF SITE D

° FOR ON THE SLOPE

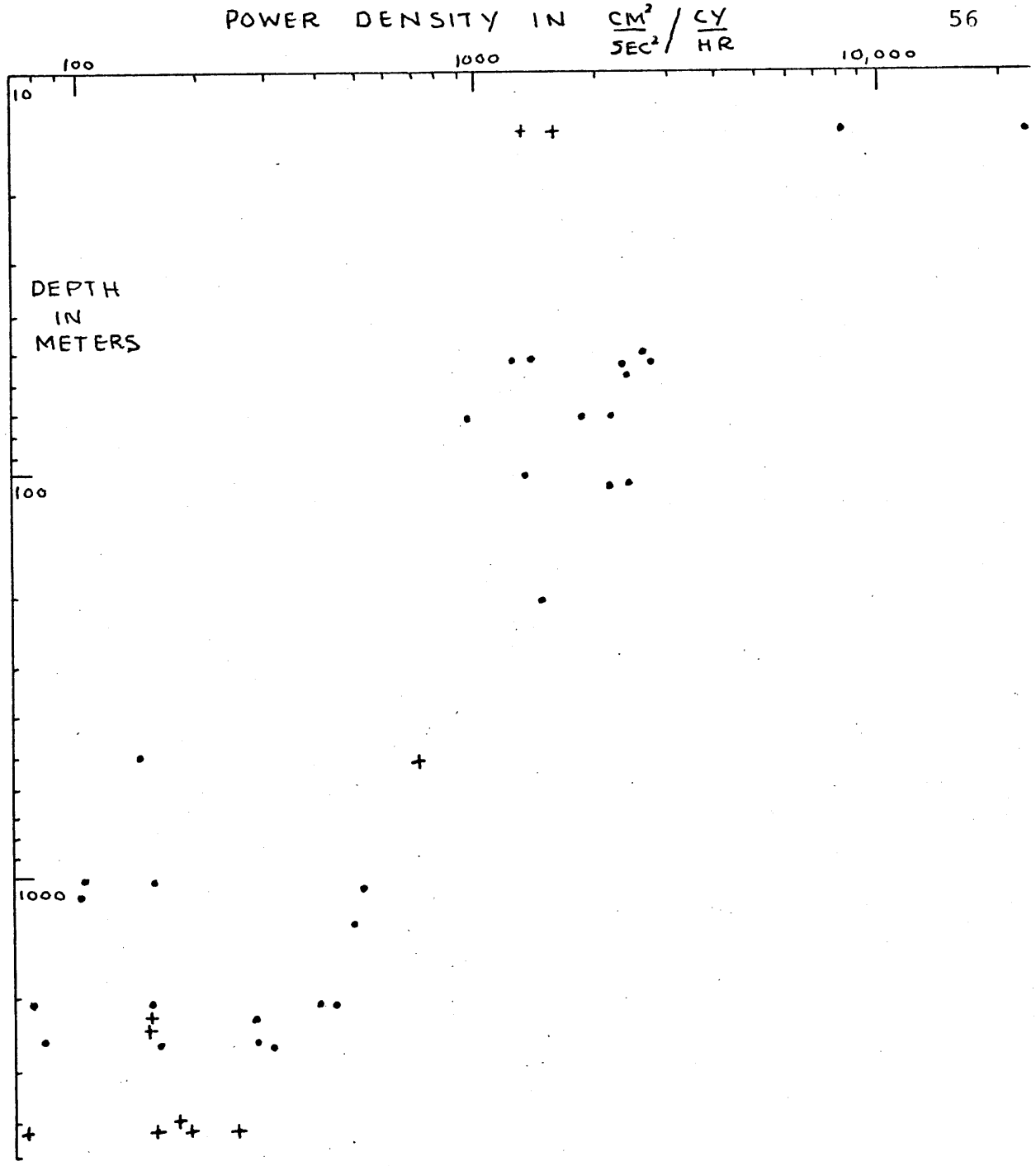

FIGURE 12

M_2 NORTH POWER DENSITIES

• FOR SITE D

+ FOR SOUTH OF SITE D

For the barotropic tide, horizontal velocities should be independent of depth. The barotropic tide is presumedly always present, so the lowest M_2 power density might be a reasonable upper bound on the barotropic M_2 power density. Of the power densities for all records (including those omitted from Table 6) six have power densities below 100 $\left(\frac{\text{cm}}{\text{sec}}\right)^2 / \frac{\text{cycle}}{\text{hour}}$. Among these six are u and v components from Site D and non-Site D records. Apparently, then, the barotropic tide contributes a small portion of the M_2 internal tide energy in these records, even at great depths. The M_2 internal tide seen here is mostly baroclinic.

The distribution of power density versus depth was found to resemble that of the Brunt-Vaisala frequency. Webster (1969) shows total kinetic energy versus depth for 25 records at Site D and compares this to a line fitted through seasonal averages of Brunt-Vaisala frequency at Site D, finding log-log eyeball agreement. The seasonal averages in Webster's paper are almost identical below 100 meters, presumedly the limit of the seasonal thermocline. Figures 13, 14, and 15 show plots of Site D Brunt-Vaisala frequency values received from Dr. William Schmitz. The shallowest value in each case is actually at one meter and off the graph. The Brunt-Vaisala frequen-

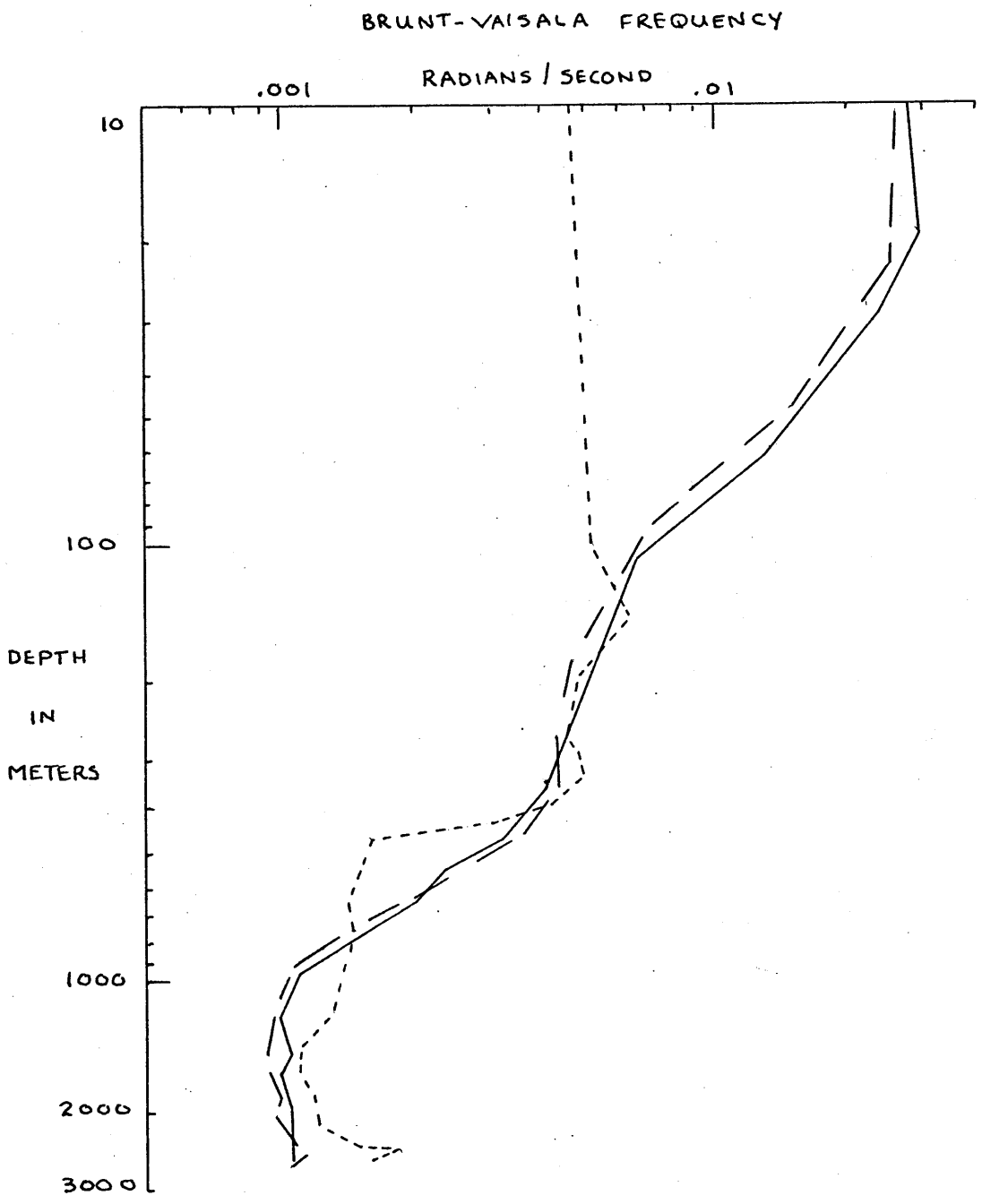

FIGURE 13

BRUNT-VAISALA FREQUENCIES FOR SITE D

—— AT 38° 59' N, 70° 00' W ON AUGUST 18, 1965

— — AT 39° 10' N, 70° 33' W ON JULY 24, 1963

- - - - AT 39° 18' N, 70° 04' W ON FEBRUARY 27, 1967

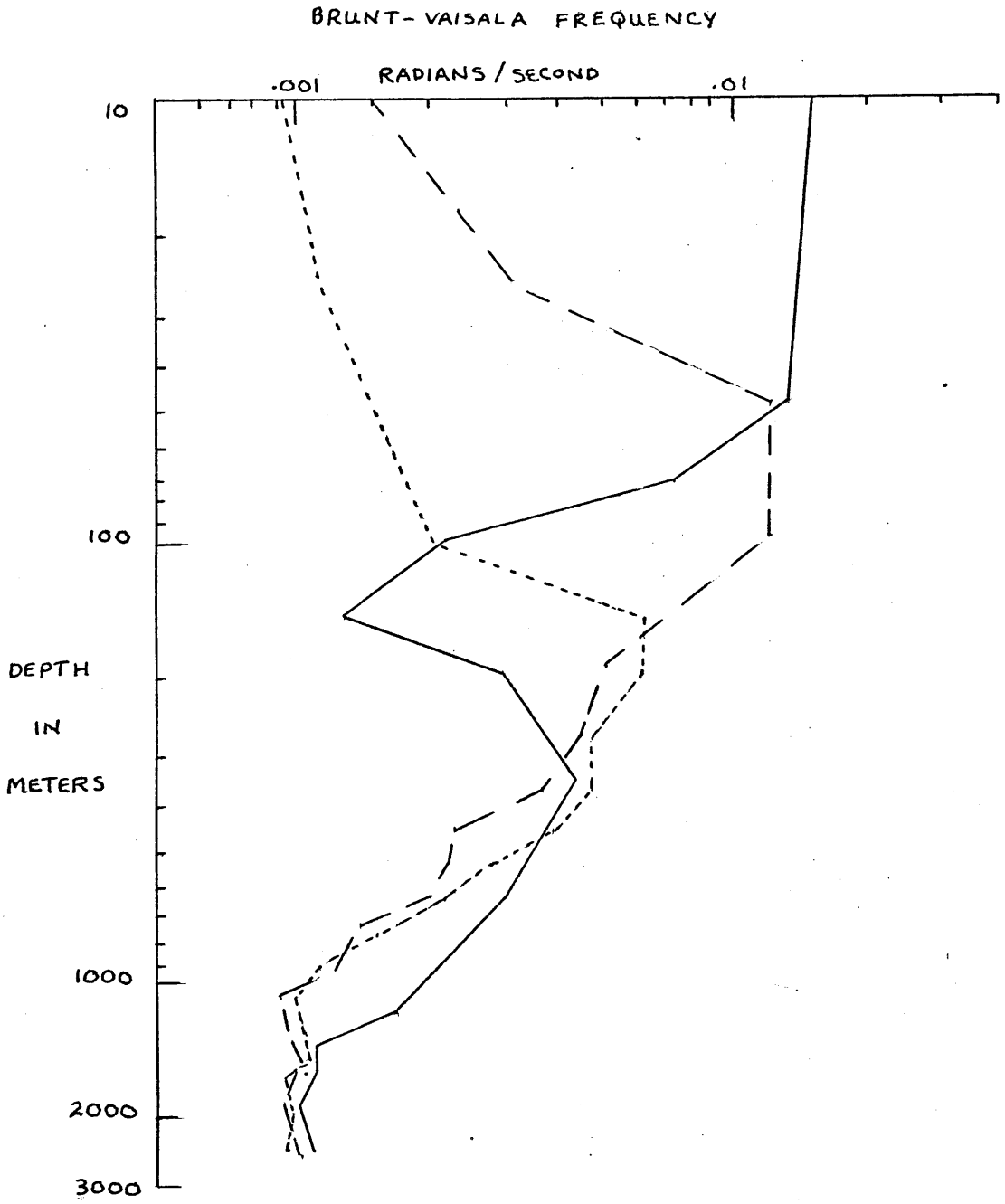

FIGURE 14

BRUNT-VAISALA FREQUENCIES FOR SITE D

——— AT 39°01'N, 70°02'W ON JUNE 18, 1967

— — AT 39°25'N, 70°00'W ON DECEMBER 30, 1965

- - - - AT 39°15'N, 70°01'W ON APRIL 22, 1965

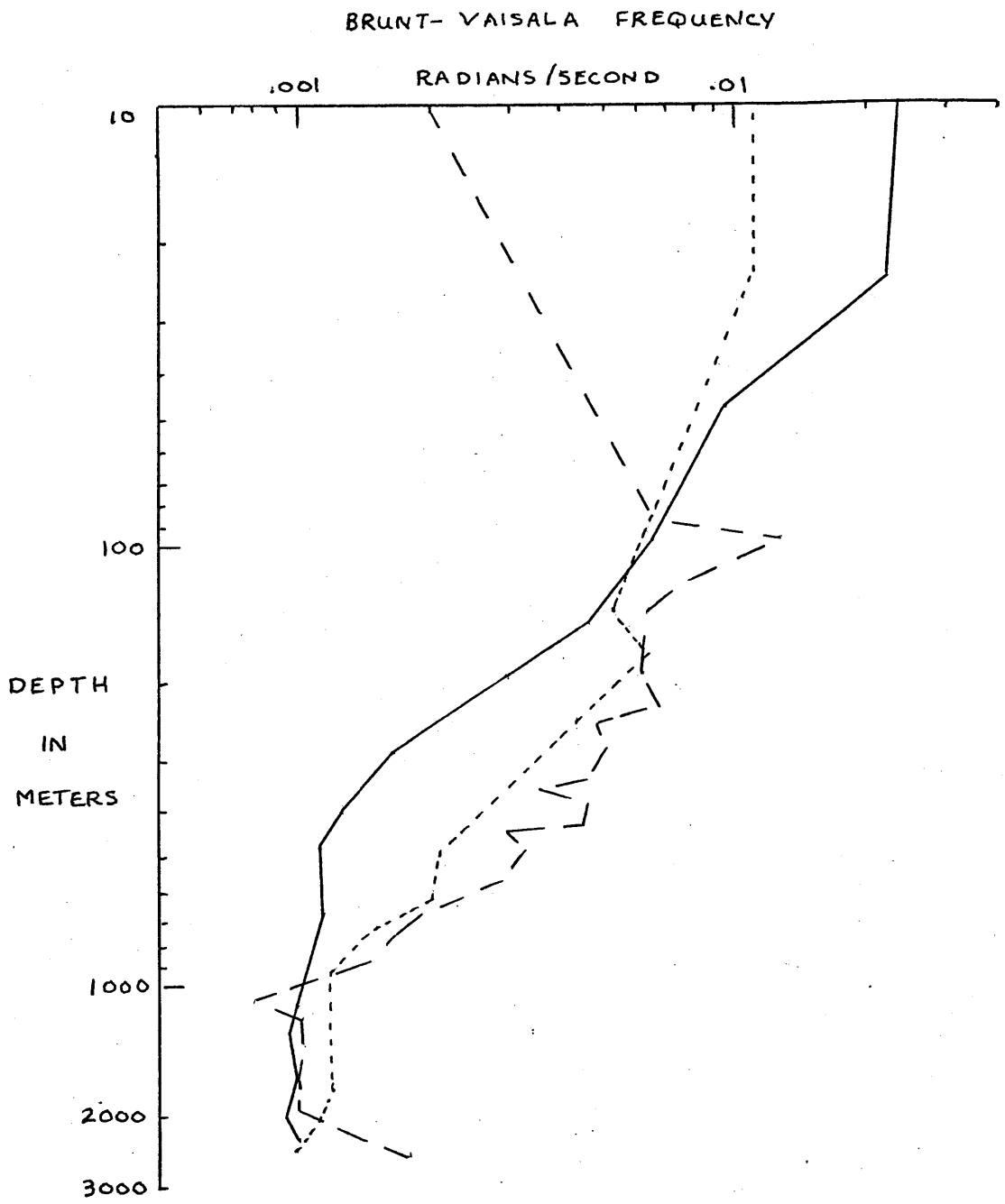

FIGURE 15

BRUNT-VAISALA FREQUENCY FOR SITE D

——— AT 39° 20' N, 69° 58' W ON OCTOBER 6, 1965

— — AT 39° 18' N, 70° 05' W ON DECEMBER 7, 1966

- - - - - AT 39° 15' N, 70° 01' W ON APRIL 28, 1965

cies for one of the stations shown here were recomputed with a computer program using sound velocity and another using specific volumes brought adiabatically to the mean pressure. The values from the sound velocity program agreed closely with the ones received and used here. The programs gave different values but very similarly shaped curves. The curves from the stations used in Figures 13 - 15 show a tendency to be similar below 100 meters.

Site D east and north velocity power densities are shown in Figures 16 and 17 with Brunt-Vaisala frequency times an arbitrary constant. The particular Brunt-Vaisala frequencies chosen are from cruise 128, station 1922 of the Crawford, the connected line in Figure 13. Both shallow records on the plots are from the summer, the season of station 1922. The power density values at Site D have too much spread to be fit or explained by one line, but the fit has a generally pleasing look, except that power densities at around 500 meters do not appear much larger than those below 500 meters. The WKBJ approximation says that u and v should go like $\sqrt{N}$ for internal waves (MUNK and PHILLIPS, 1970) and hence like N for power densities, which were calculated by squaring u and v amplitudes. Hence, the similar depth dependence of the Brunt-Vaisala frequency and u and v power densities at Site D indicates that the M_2 internal tide at Site D is governed by

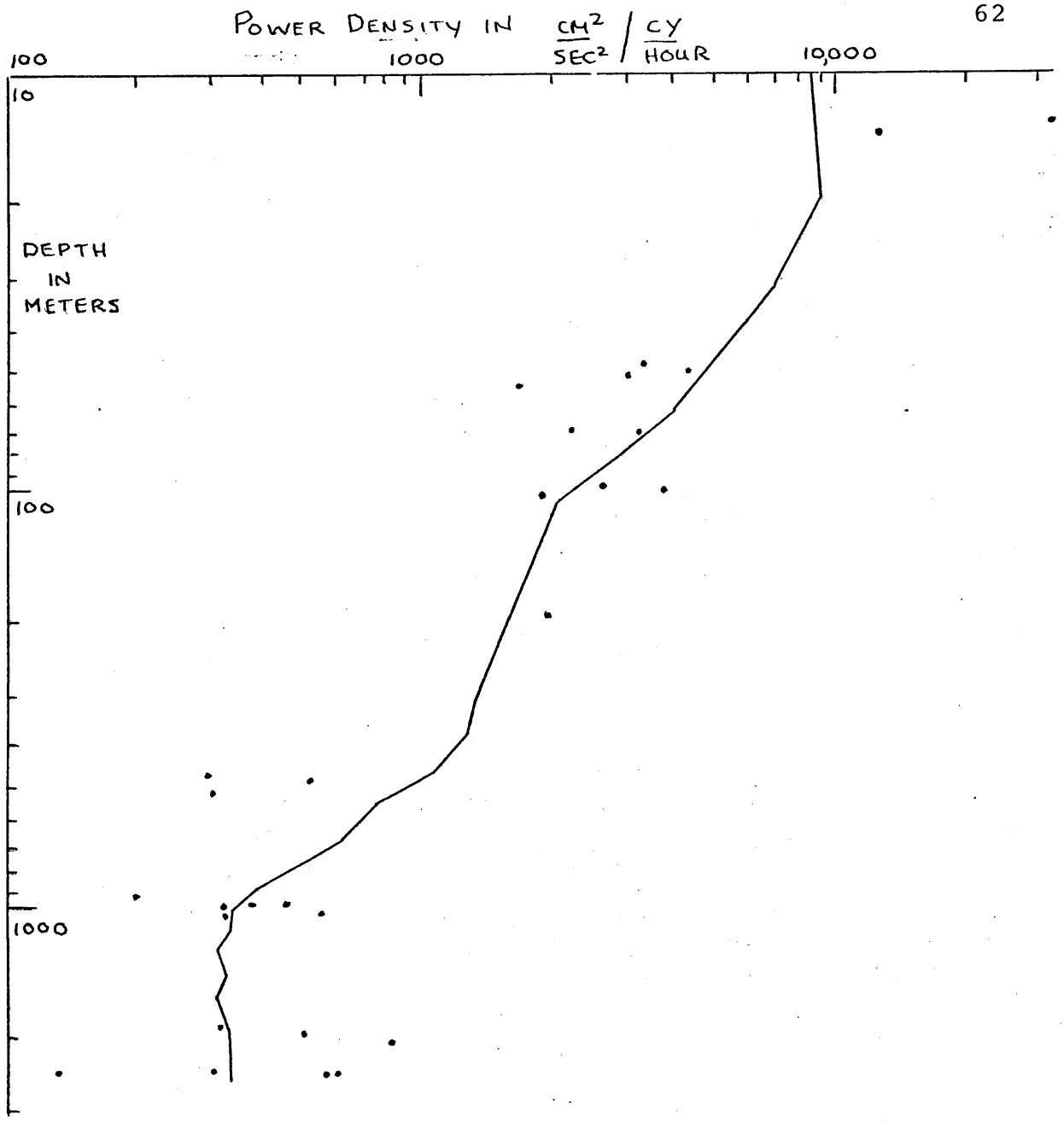

FIGURE 16

SITE D EAST POWER DENSITIES AND BRUNT-VAISALA FREQUENCY

The line here is the solid line in Figure 13 arbitrarily superimposed.

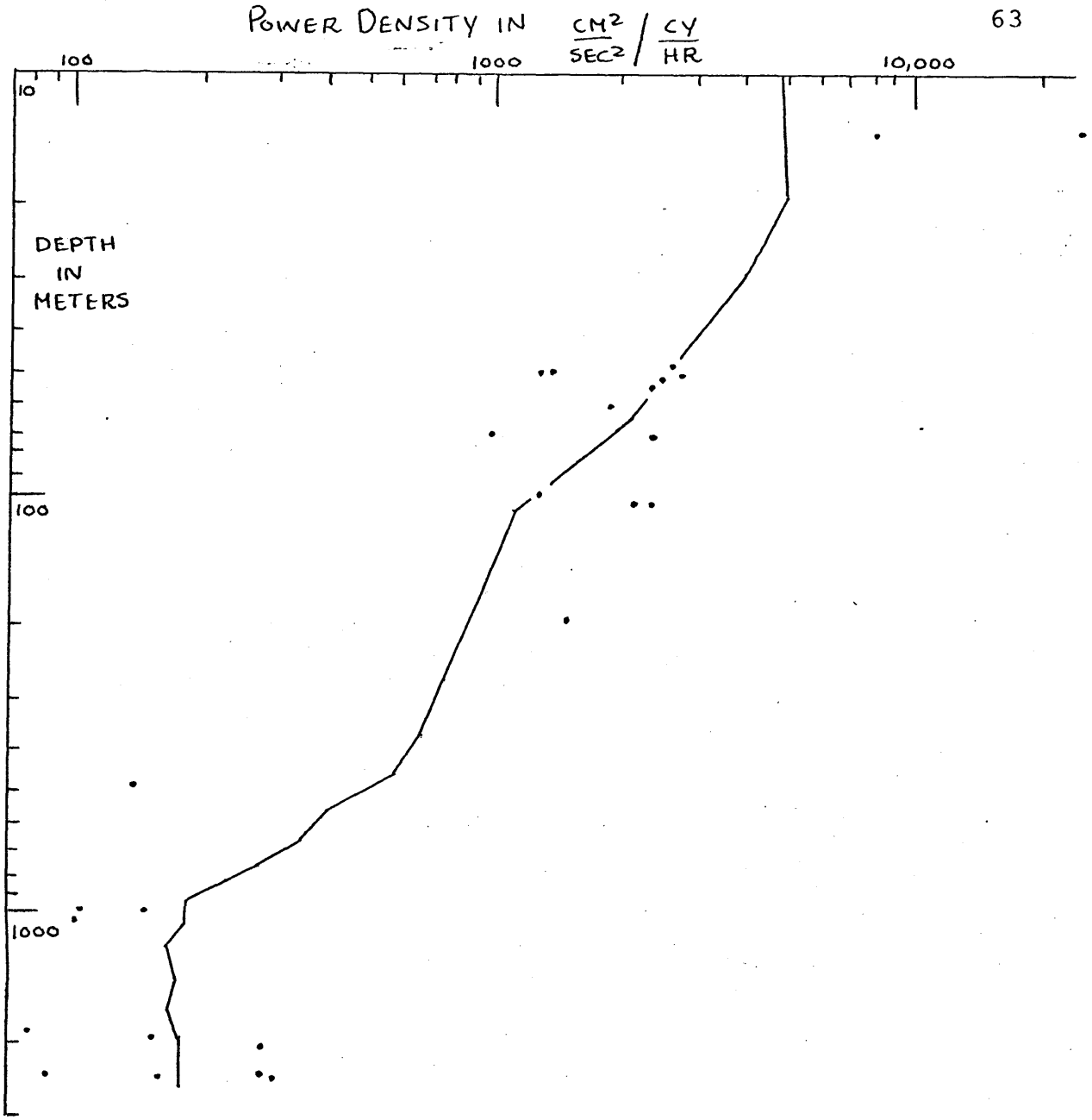

FIGURE 17

SITE D NORTH POWER DENSITIES AND BRUNT-VAISALA FREQUENCY

-The line here is the solid line in Figure 13 arbitrarily superimposed.

internal wave dynamics.

The plots show that Brunt-Vaisala frequencies can be quite variable in the upper layers so that one might try to explain the variability in the power densities in the upper layer of Site D this way. However, spring and winter power densities in the upper layer showed no tendency to be smaller than summer and fall measurements at about the same depth as the Brunt-Vaisala frequencies do. Since the Brunt-Vaisala frequency seems fairly uniform from station to station below 1000 meters at Site D, it would be hard to explain the much greater variability in M_2 power densities there by varying Brunt-Vaisala frequencies.

The u and v power densities for the records south of Site D also behave similarly to the Brunt-Vaisala frequency there. Figures 18 and 19 show Brunt-Vaisala frequencies for south of Site D. These were calculated from station data from Dr. William Schmitz and the Woods Hole Oceanographic institution files. Once again values at one meter are off the graphs. All of these were calculated with both sound velocity and specific volume programs. Again the programs gave different answers but very similarly shaped curves. The ones shown here are the Brunt-Vaisala frequencies from the sound velocity program. The ratios of the power density values at 14 meters to

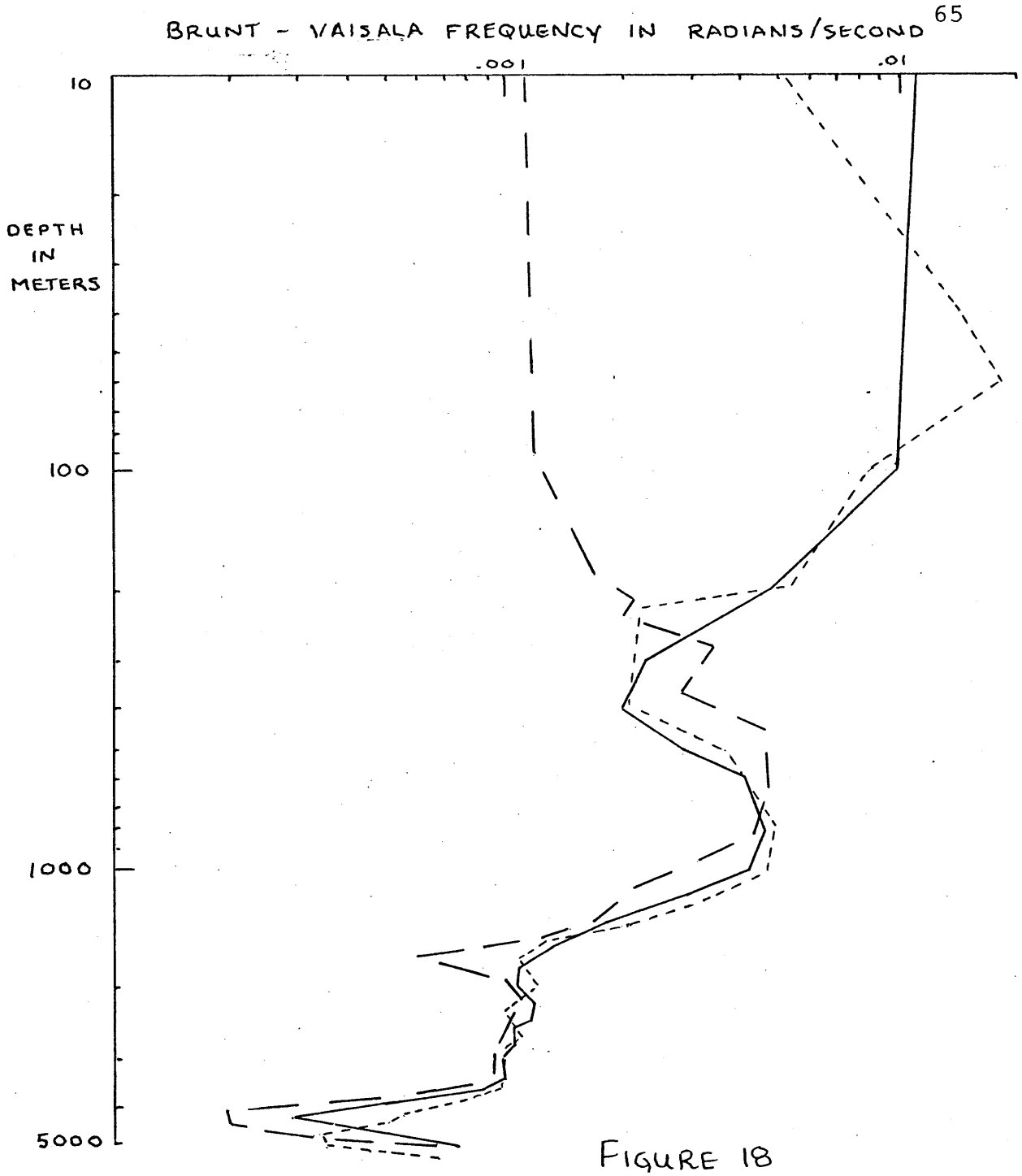

FIGURE 18

BRUNT - VAISALA FREQUENCIES AROUND 34° N

——— AT 33°55′ N, 69°51′ W ON JUNE 7, 1970

— — AT 34°00′ N, 70°10′ W ON MARCH 1, 1970

----- AT 34°00′ N, 69°58′ W ON OCTOBER 10, 1970

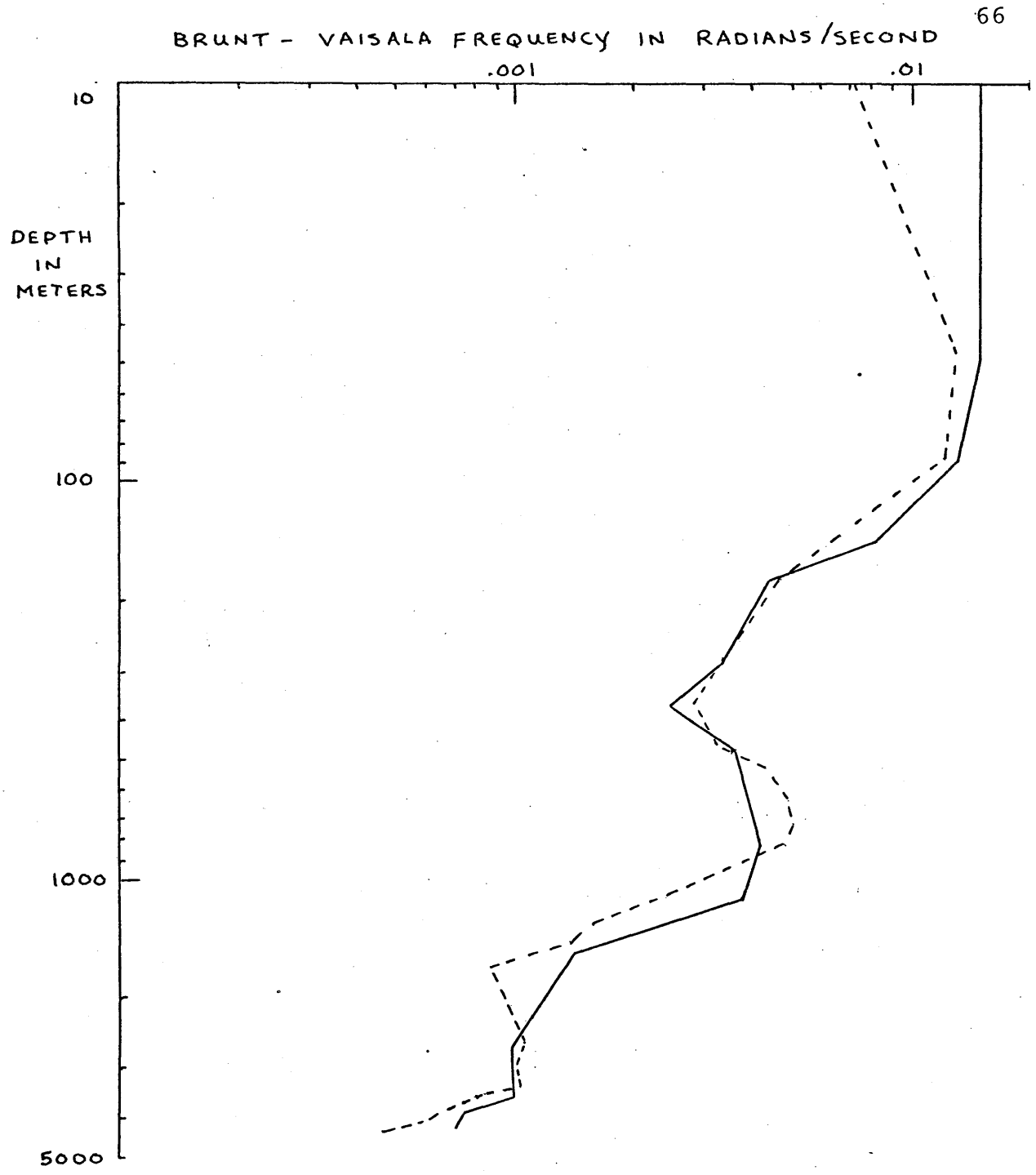

FIGURE 19

BRUNT-VAISALA FREQUENCIES AROUND 34° N

——— AT 34°01' N, 70°05' W ON AUGUST 19, 1969

- - - - - - AT 34°03' N, 70°03' W ON OCTOBER 27, 1971

those deeper are smaller south of Site D than at Site D. This could be because the Brunt-Vaisala frequencies south of Site D do not rise much above the values at 100 meters as the summer Site D values do. The power density values south of Site D do not reflect the fall of the Brunt-Vaisala frequency at depths below 2000 meters. Possibly what is being seen from 2000 meters down is mostly barotropic tide and noise. The rise in values from above 2000 meters, though, is consistent with a dependence on the Brunt-Vaisala frequency.

The dominance of east-west velocities seen earlier in the Fourier coefficient amplitudes and tidal ellipses appears also in the power densities. The ratio of v power density to u power density in the same record for the values in Table 6 averages .39 for Site D records below 210 meters, .83 for Site D records above 210 meters, and 1.11 for records south of Site D. This is shown graphically in Figure 20. There is a possibility that the choice of which M_2 power densities to include in Table 6 contributed to this result, but the ones not considered reliable enough for Table 6 go much the same way. Of those, all south of Site D and in the upper layers of Site D have north to east power density ratios above one, while six of the seven in deep Site D have ratios less than .65, the other being 1.50. Webster (1969) found

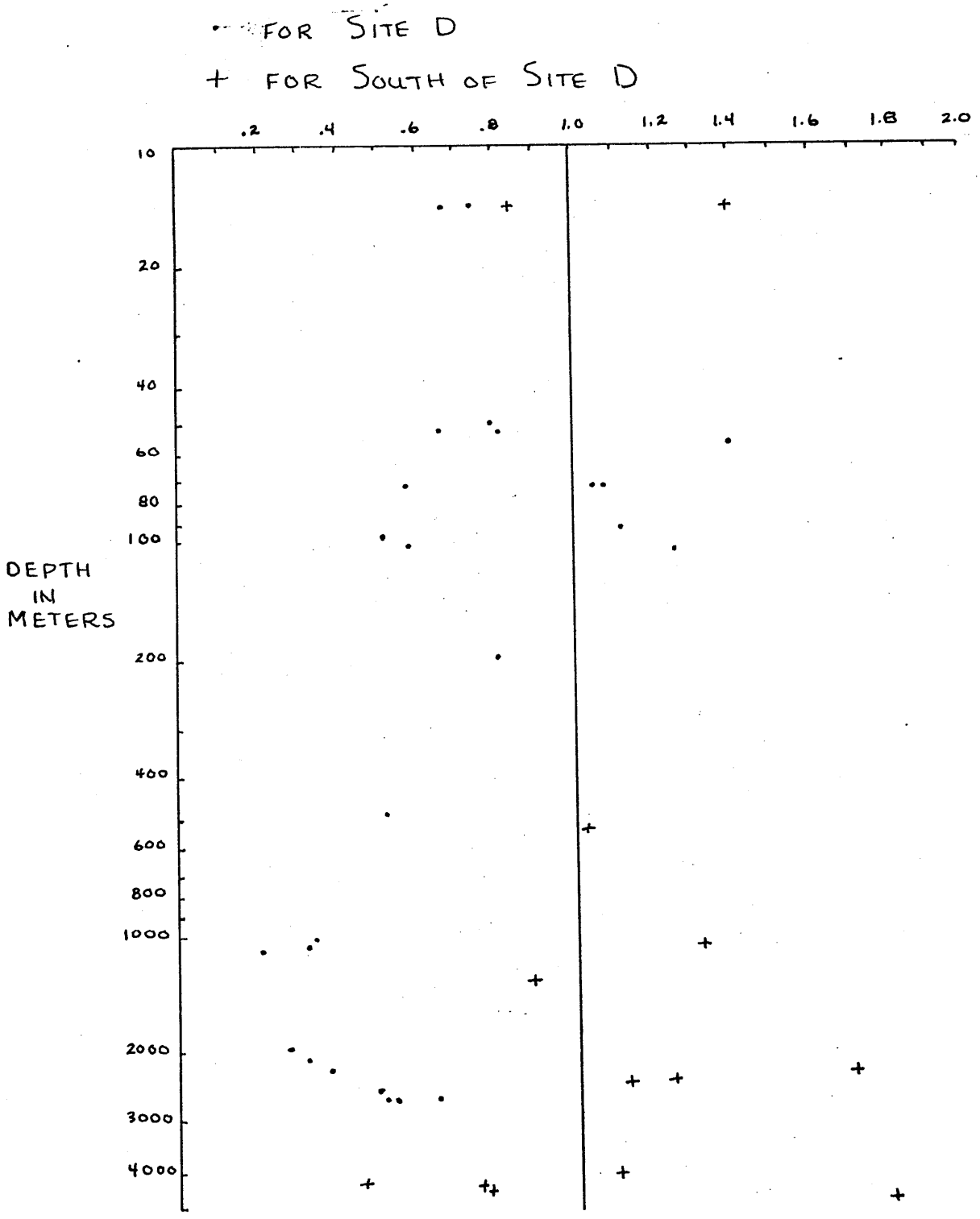

FIGURE 20

RATIOS OF NORTH TO EAST POWER DENSITIES

that his low frequency north-south fluctuations at Site D seemed to be suppressed below 200 meters. He attributed this to the continental slope, which forms a east-west wall below 200 meters about 50 to 70 kilometers north of Site D. Webster (1969) said, though, that for periods shorter than a day he saw isotropy of u and v intensities, using 8 hour and inertial period oscillations as examples. The inertial power densities calculated for the section on correlations in this paper also showed east-north isotropy. The ratios averaged .98 for shallow Site D, 1.09 for deep Site D, and 1.01 for south of Site D. As pointed out by Wunsch (personal communication), one possible difference between the effect of the shelf on inertial oscillations and M_2 internal tides is the β -trapping effect on the inertial oscillations (MUNK and PHILLIPS, 1968). The north to east power density ratios of about .4 in deep Site D are inconsistent with a plane wave coming from the north but are consistent with a plane wave coming from the east or west.

It should be remembered that the continental slope to the north of Site D is not the perfectly vertical wall that it has been represented as here when talking about the generation of the internal tides at the edge of the shelf or the interaction of the M_2 internal tide with the slope. The angle of the slope at any point

determines whether internal tides are transmitted up the slope, and points of transition between the reflecting and transmitting slope are expected points of generation of internal tides (WUNSCH, 1969). There may be several such critical changes of angle on the slope, so that when the M_2 internal tide at Site D is found to be inconsistent with a single plane wave coming from the north, this hardly disproves the general hypothesis of generation of M_2 internal tides north of Site D at the slope.

VI. CORRELATIONS

In order to investigate the possibility of energy flow from the M_2 internal tide to other parts of the spectrum, correlation coefficients were determined for tidal power densities versus short, inertial, and long period variations. In all cases this was u versus $\dot{u}$ and v versus v. The other power densities for a record were calculated with the same number of points as had been used for the tidal power densities for that record. Since the time step for each record was two hours, the cutoff frequency was 1/4 cycles/hour, which gives 4 hours as the shortest period for which Fourier coefficients were calculated. The long period values were taken from the longest periods calculated, not including the mean. The inertial points were found by looking for the biggest concentration of power somewhere near $\sin\theta/12$ cycles per hour, where θ is the latitude.

It should be pointed out that the numerical methods used here have sufficient resolution so that a fluctuation at one of the periods will not significantly affect the Fourier transform values at any of the other three frequencies, which would introduce spurious correlations. This is essentially shown by the rapid fall of the equilibrium tide Fourier coefficient amplitudes in Figure 2.

As a numerical example, a unit sine wave of 19 hour period sampled 512 times every two hours (1024 hours = $42.\overline{66}$ days) shows up as Fourier coefficient amplitudes of 0.983 at 18.96 hours, 0.005 at 12.49 hours, 0.001 at 4 hours, and 0.000 at 1024 hours.

The correlation coefficient, r, is defined as

$$\frac{\sum (X_i - \bar{X})(Y_i - \bar{Y})}{\sqrt{[\sum (X_i - \bar{X})^2][\sum (Y_i - \bar{Y})^2]}} =$$

$$\frac{N\sum X_i Y_i - (\sum X_i)(\sum Y_i)}{\sqrt{[N\sum X_i^2 - (\sum X_i)^2][N\sum Y_i^2 - (\sum Y_i)^2]}} ,$$

where "i" ranges from 1 to N and $\bar{X}$ denotes the average of the N X-values. For points on a straight line with positive slope, r = +1, a perfect positive correlation. For points on a straight line with negative slope, r = -1, a perfect negative correlation. For points with no tendency toward a linear fit, r = 0, no correlation. By definition r is always between +1 and -1. The calculated coefficients for different regions are given in Table 7.

The correlation coefficients for all records and all depths show surprisingly high, significantly non-zero correlation coefficients for tidal versus short and inertial period power densities. High correlation coefficients

in themselves, however, do not prove causation. These high correlations may reflect a similar dependence on oceanic conditions. If surface values tend to be much larger than deeper values, then the correlation coefficient will pick a positively sloped line from the low deep values to the high surface values. All four frequencies showed high power densities in the records near 14 meters. For the tidal, four hour, and inertial periods this could be explained by the high surface Brunt-Vaisala frequencies, since these three periods are in the internal gravity wave range. The few high surface values account for much of the correlation. When only records below fifteen meters are considered, all correlation coefficients drop, and only one short period correlation is significantly non-zero. Both inertial correlation coefficients are significantly non-zero still but not as large as with the fourteen meter records included. As seen in the figures of Brunt-Vaisala frequency at Site D shown earlier, the Brunt-Vaisala frequency at depths over 1000 meters tends to be fairly uniform over depth and time at Site D. So correlations between records in this region would not be expected to be dominated by underlying Brunt-Vaisala frequency dependences. The third group of correlation coefficients in Table 7 shows that correlations are down considerably

when only deep Site D records are considered. The statistically small number of records falling into this catagory, though,makes conclusions difficult.

It may be reasonable to assume that Brunt-Vaisala dependences would not contribute greatly to correlations for all meters below 1000 meters. For this group the next to last set in Table 7 shows small correlation coefficients for tidal versus 4 hour power density and moderate coefficients for both u and v at inertial period. The coefficient for inertial u versus tidal u is nearly significant at the 95% level, and the coefficient for v is significantly above .30.

Possibly in the upper layers where the powers are high there is more spreading of the tidal energy than in the deep water. This may be especially true of short period variations which may receive energy from the breaking of large M_2 internal waves. The Brunt-Vaisala frequency at depths above 100 meters is variable at Site D, but correlation coefficients were still calculated for records at Site D from depths from 52 to 108 meters. These show significant positive inertial correlations for east velocity and negative, not significantly zero four hour correlations. This may indicate a connection between M_2 and inertial powers but makes conclusions about short versus tidal power densities difficult.

The only conclusions drawn here are that most of the correlation seen when considering all records can be attributed to underlying, similar responses at the different frequencies to oceanic conditions and that in deep Site D there does not appear to be any spreading of the M_2 power to other frequenciesseen here.

TABLE 7

CORRELATION COEFFICIENTS

PERIOD	CORRELATION COEFFICIENT	NUMBER OF RECORDS	95% CONFIDENCE LIMITS LOWER	UPPER
ALL RECORDS AND ALL DEPTHS				
		EAST(u)		
SHORT	.51	45	.25	.75
INERTIAL	.88	"	.82	.95
LONG	.41	"	.15	.60
		NORTH(v)		
SHORT	.90	41	.83	.95
INERTIAL	.94	"	.90	.97
LONG	.14	"	-.15	.40
ALL RECORDS BELOW 15 METERS				
		EAST(u)		
SHORT	.33	41	.00	.50
INERTIAL	.57	"	.30	.75
LONG	.28	"	-.10	.45
		NORTH(v)		
SHORT	.47	37	.15	.65
INERTIAL	.61	"	.30	.75
LONG	.10	"	-.25	.35
SITE D RECORDS BELOW 1000 METERS				
		EAST(u)		
SHORT	.21	12	-.40	.75
INERTIAL	.13	"	-.45	.65
LONG	-.12	"	-.60	.50
		NORTH(v)		
SHORT	-.24	10	-.70	.45
INERTIAL	.30	"	-.40	.75
LONG	.25	"	-.45	.70

PERIOD	CORRELATION COEFFICIENT	NUMBER OF RECORDS	95% CONFIDENCE LIMITS LOWER	UPPER
		NON-SITE D RECORDS BELOW 1000 METERS		
		EAST(u)		
SHORT	.22	14	-.30	.60
INERTIAL	.35	"	-.20	.75
LONG	-.32	"	-.70	.20
		NORTH(v)		
SHORT	-.19	12	-.60	.35
INERTIAL	.66	"	.20	.85
LONG	.67	"	.20	.85
		ALL RECORDS BELOW 1000 METERS		
		EAST(u)		
SHORT	.15	26	-.20	.50
INERTIAL	.34	"	-.05	.70
LONG	-.35	"	-.70	.05
		NORTH(v)		
SHORT	-.05	22	-.35	.35
INERTIAL	.64	"	.30	.85
LONG	.49	"	.10	.75
		SITE RECORDS FROM 52 TO 108 METERS		
		EAST(u)		
SHORT	-.36	10	-.75	.35
INERTIAL	.70	"	.10	.90
LONG	.10	"	-.55	.60
		NORTH(v)		
SHORT	-.52	12	-.85	.20
INERTIAL	.32	"	-.40	.75
LONG	-.25	"	-.75	.45

VII. CONCLUSIONS

The Fourier coefficients of east and north horizontal water velocity in 58 moored current meter records from the western North Atlantic were inspected for the presence of internal tides. Evidences of internal tides at all the main tidal forcing frequencies were found. The M_2 internal tide, though, was usually dominant and was the only internal tide found in a good number of the records. Four measures of the internal tide were shown here - Fourier coefficients, admittances, tidal ellipses, and power densities.

In all of these measures the variability of the M_2 internal tide could be seen. In some records there was an unmistakable M_2 signal, while in others no sign of the M_2 internal tide could be found. As seen in moorings 189 and 212, the internal tide in the same area during the same season of different years can show different characteristics. On mooring 189 the east component of the M_2 internal tide near 1000 meters was larger than the semidiurnal fluctuations near 2000 meters and nearly in phase with the tide at 100 meters. On mooring 212 the M_2 east fluctuations near 1000 meters were smaller than at 2000 meters and nearly 180° out of phase with the tide at 50 meters. For both 212 and 189 the admittance phase

for the east component of the shallowest meter was about 300°, a value which showed up in some of the other Site D records. This variability of the semidiurnal tide is consistent with the findings of other investigators (HECHT and HUGHES, 1971). The differences in Fourier coefficient amplitudes did not disappear with the equilibrium tide normalization. Including neighboring frequencies in the power density calculations might be expected to reduce the variability some, but the M_2 power densities showed wide variations.

Despite the variability of the M_2 internal tide, there appeared to be a definite depth dependence. In most cases M_2 Fourier coefficient and admittance amplitudes on the same mooring were larger in shallower records. This appeared again in the power densities. Comparison of the depth dependences of the power densities and the Brunt-Vaisala frequency showed striking similarity. Having power densities roughly proportional to the Brunt-Vaisala frequency is consistent with the behavior of non-zero mode internal gravity waves, since the WKBJ approximation shows that u and v should go roughly like the square root of the Brunt-Vaisala frequency for internal gravity waves. The findings of Fofonoff (1969) would suggest such behavior for the M_2 internal tide at Site D, since the frequency of the semidiurnal

oscillations there is between the local inertial and maximum Brunt-Vaisala frequencies. This internal wave-like behavior of the semidiurnal internal tide is consistent with the findings of other investigators (HECHT and HUGHES, 1971; LEE and COX, 1966).

The surface tide appeared to contribute little to most of the internal tides seen here. The surface tide would be expected to be fairly constant over time and should have velocities in the horizontal independent of depth. The low power densities seen in several of the records indicate a low upper bound on the power density contributed by the surface, barotropic tide. Along with the dependence of the amplitudes on the Brunt-Vaisala frequency, this indicates that the semidiurnal internal tide in the western North Atlantic is composed largely of baroclinic internal gravity waves.

The velocities at Site D were found to be more east-west than north-south, especially in the deep records. This anisotropy of the horizontal motions did not show up south of Site D. The dominance of the east-west velocities in deep Site D may be due to the influence of the continental shelf to the north of Site D (WEBSTER, 1969).

Attempts at finding an indication of whether the Rattray(1960 and 1969) or Cox and Sandstrom(1962) model of the generation of the M_2 internal tide fit the M_2

internal tides seen here proved inconclusive. The Rattray model of generation of internal tides at the edges of the continental shelves would suggest a generation of the Site D internal tides to the north of Site D. This would suggest an attenuation of amplitudes to the south, but no latitudinal variation of the Site D M_2 internal tide was found, possibly due to the variability over time of the internal tide. The motions seen here do not fit the simple model of a plane wave generated to the north (or any direction), but this is not a proof or disproof of either of the models.

Correlation coefficients were calculated for an indication on the possibility that internal tides feed energy to other frequencies. The correlations between power densities at M_2 period and those at inertial and four hour periods for all records and depths were found to be surprisingly high. These high correlations are probably more an indication of similarity in response at these frequencies to oceanic conditions than feeding of tidal energy. Since the tidal, inertial, and four hour periods are all in the range of periods expected to be governed by internal wave dynamics (FOFONOFF, 1969), what is probably being seen here is the tendency for values in the surface layers to be large at these three frequencies. Correlations in deep Site D where the Brunt-Vaisala

frequency is fairly constant over depth and time showed no large correlations.

The main conclusion that can be drawn here is that the semidiurnal internal tide in the western North Atlantic seems to be composed mostly of baroclinic internal gravity waves.

APPENDIX I

THE RELATION BETWEEN ELLIPTICITY AND CLOCKWISE CHARACTER OF ELLIPSES

Let $u = A_1\cos(\omega t) + B_1\sin(\omega t)$ and

$v = A_2\cos(\omega t) + B_2\sin(\omega t)$.

The total velocity vector, $\underline{u} = (u,v)$, sweeps out an ellipse. Let plus (+) denote counterclockwise and minus (-) denote clockwise. The total velocity can be written in complex notation as

$$u + iv = u_+e^{i\omega t} + u_-e^{-i\omega t} .$$

Substituting the expressions for u and v from above, using the relation $e^{ix} = \cos(x) + i\sin(x)$, and equating sine and cosine terms gives two equations for u_+ and u_- which have the solutions

$$u_+ = \frac{1}{2}\,[(A_1+B_2) + i(A_2-B_1)] = |u_+|e^{i\theta_+} \text{ and}$$

$$u_- = \frac{1}{2}\,[(A_1-B_2) + i(A_2+B_1)] = |u_-|e^{i\theta_-}$$

(GONELLA, 1971). Here the notation $|x + iy|$ is the usual modulus of the complex number, $\sqrt{x^2 + y^2}$. So $|u_+|$ and $|u_-|$ are the amplitudes of the counterclockwise and clockwise components of the ellipse. It can be shown that

$|u_+|$ and $|u_-|$ are undependent of the orientation of the ellipse with respect to the axes. Let |major| and |minor| be 1/2 the lengths of the major and minor axes or the velocity amplitudes at the axes. If R is the lesser of $|u_+|/|u_-|$ and $|u_-|/|u_+|$, then

$$\frac{|\text{minor}|}{|\text{major}|} = \frac{1 - R}{1 + R} . \qquad (*)$$

That equation (*) holds can be shown as follows. First consider the special case of a counterclockwise ellipse with major axis east-west. Not considering starting position, u and v can then be represented as

$$u = A_1 \cos(\omega t) \quad \text{and}$$

$$v = B_2 \sin(\omega t) ,$$

where $A_1 > 0$, $B_2 > 0$, and $A_1 > B_2$. In this case

$$|u_+| = A_1 + B_2 \quad , \text{and}$$

$$|u_-| = A_1 - B_2 \quad , \text{giving}$$

$$\frac{1 - R}{1 + R} = \frac{1 - \dfrac{A_1 - B_2}{A_1 + B_2}}{1 + \dfrac{A_1 - B_2}{A_1 + B_2}} = \frac{B_2}{A_1} = \frac{|\text{minor}|}{|\text{major}|} .$$

Since any counterclockwise ellipse can be obtained by rotation of an ellipse of the above special kind and $|u_+|$, $|u_-|$, |minor|, and |major| are independent of orientation, the truth of (*) for the special case implies the truth

of (*) for any counterclockwise ellipse. Changing the sign of B_1 shows that (*) holds likewise for any clockwise ellipse.

APPENDIX II

TIDAL ELLIPSES FOR A PLANE WAVE

If the internal tide is considered a plane wave with parallel wave fronts in the direction α and ω is greater than f, then the tidal ellipse will have its major axis in the direction $\alpha + 90°$ and will have axes in the ratio f/ω. Here u and v are the east and north velocities. The positive x-axis is taken as east with positive y north. P is the reduced pressure. The inertial and tidal frequencies are f and ω. Now u and v must at least satisfy the equations

$$\frac{\partial u}{\partial t} - fv = -\frac{\partial P}{\partial x} \qquad (*)$$

and $$\frac{\partial v}{\partial t} + fu = -\frac{\partial P}{\partial y} .$$

Looking for periodic solutions, set $u = u \cdot e^{-i\omega t}$, $v = v \cdot e^{-i\omega t}$, and $P = P \cdot e^{-i\omega t}$, giving

$$-i\omega u - fv = -\frac{\partial P}{\partial x} \qquad (**)$$

and $$-i\omega v + fu = -\frac{\partial P}{\partial y} .$$

If the internal tide is thought of as a plane wave with wave fronts at an angle α, then the partial derivative of P in the direction α is zero so that

$$\frac{\partial P}{\partial x}\cos(\alpha) + \frac{\partial P}{\partial y}\sin(\alpha) = 0.$$

Along with equations (**) this implies

$$\frac{u}{v} = \frac{f\cos(\alpha) + i\omega\sin(\alpha)}{f\sin(\alpha) - i\omega\cos(\alpha)} .$$

So to within a constant multiple, u and v can be represented as

$$\begin{aligned} u &= f\cos(\alpha)\cos(\omega t) + \sin(\alpha)\sin(\omega t) \\ \text{and} \quad v &= f\sin(\alpha)\cos(\omega t) - \cos(\alpha)\sin(\omega t) \end{aligned} \qquad (***)$$

for some arbitrary time origin. The u and v in (***) can be represented as

$$\begin{pmatrix} u \\ v \end{pmatrix} = \begin{pmatrix} \cos(\alpha) & -\sin(\alpha) \\ \sin(\alpha) & \cos(\alpha) \end{pmatrix} \begin{pmatrix} f\cos(\omega t) \\ -\omega\sin(\omega t) \end{pmatrix}$$

which is just the ellipse

$$\begin{pmatrix} u \\ v \end{pmatrix} = \begin{pmatrix} f\cos(\omega t) \\ -\omega\sin(\omega t) \end{pmatrix}$$

rotated counterclockwise by the angle α. If $\omega > f$, then this latter ellipse is a clockwise ellipse with major axis at $\pi/2$ and ratio of minor to major axis of f/ω. Therefore with $\omega > f$ the ellipse of equations (***) is a clockwise ellipse with major axis at $\alpha + \pi/2$ and with axes in the ratio f/ω. This can be checked by substituting $u = A_1\cos(\omega t) + B_1\sin(\omega t)$ and $v = A_2\cos(\omega t) + B_2\sin(\omega t)$ into equations (*). The pressure relation then gives an equation in $\sin(\omega t)$ and $\cos(\omega t)$ which gives, say, A_2 and

B_2 in terms of A_1 and B_1. It can be shown that an ellipse determined by such coefficients is tilted at an angle $\alpha + \pi/2$ and has axes in the ratio f/ω.

APPENDIX III

BAND-PASSING

In looking for internal tides, investigators have sometimes tried band-passing around the frequency of interest. The effect of band-passing on the signal, though, is to introduce apparent oscillations at the frequency of interest into a time plot of the band-passed signal. Now with the use of the fast Fourier transform, a usable band-pass filter can be performed by doing the transform, setting all transform values outside the desired frequency range to zero, and then doing an inverse transform. Now all frequencies outside of the desired band have been suppressed.

It is possible to find an expression for the new signal in terms of the original. Take f(t) to be the original signal. The Fourier transform of f(t) can be defined as

$$F[f(t)] = \hat{f}(s) = \int_{-\infty}^{\infty} f(t) e^{-2\pi i s t} dt \ .$$

Passing only frequencies between $s = b + \frac{a}{2}$ and $s = b - \frac{a}{2}$ amounts to multiplying f(s) by the function

$$\pi \left(\frac{s - b}{a}\right) + \pi \left(\frac{s + b}{a}\right) \ ,$$

where $\Pi(x) = \begin{cases} 1 & , |x| < 1/2 \\ 1/2 & , |x| = 1/2 \\ 0 & , |x| > 1/2 \end{cases}$.

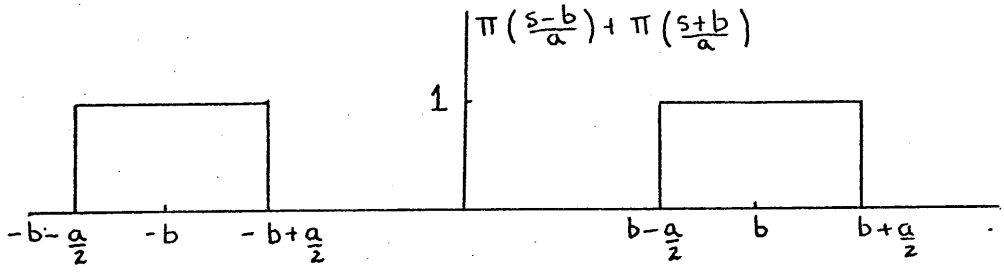

Now the inverse transform of the band-passed transform is

$$F^{-1}\left\{\hat{f}(s)\left[\Pi\left(\frac{s-b}{a}\right) + \Pi\left(\frac{s+b}{a}\right)\right]\right\} .$$

At this point some easily proven properties of Fourier transforms are needed (BRACEWELL, 1965).

$$F^{-1}[(g+h)(s)] = \hat{g}^{-1}(t) + \hat{h}^{-1}(t).$$

$$F^{-1}[g(s-a)] = e^{2\pi i a s}\,\hat{g}^{-1}(t).$$

$$F^{-1}[g(as)] = \frac{1}{|a|}\,\hat{g}^{-1}(t/a).$$

$$F^{-1}[(gh)(s)] = \hat{g}^{-1} * \hat{h}^{-1}(t) = \int_{-\infty}^{\infty} \hat{g}^{-1}(u)\,\hat{h}^{-1}(t-u)\,du$$

The operation * is called convolution.

$$F^{-1}[\Pi(s)] = \mathrm{sinc}(t) = \frac{\sin(\pi t)}{\pi t} .$$

Using these relations gives

$$F^{-1}\left\{f(s)\left[\Pi\left(\frac{s-b}{a}\right) + \Pi\left(\frac{s+b}{a}\right)\right]\right\} =$$

$$F^{-1}[\hat{f}(s)]*F^{-1}\left[\pi\left(\frac{s-b}{a}\right)\right] + F^{-1}[\hat{f}(s)]*F^{-1}\left[\pi\left(\frac{s+b}{a}\right)\right] =$$

$$f(t)*ae^{2\pi ibt}\text{sinc}(at) + f(t)*ae^{-2\pi ibt}\text{sinc}(at) =$$

$$af(t)*\text{sinc}(at)\left(e^{2\pi ibt} + e^{-2\pi ibt}\right) =$$

$$af(t)*\left[\frac{2\sin(\pi at)\cos(2\pi bt)}{\pi at}\right] =$$

$$\frac{2}{\pi} f(t)*\left[\frac{\sin(\pi at)\cos(2\pi bt)}{t}\right] .$$

The $\cos(2\pi bt)$ and $\sin(\pi at)$ terms will be expected to introduce periodicities into the signal. Just how a convolution will do this is most easily seen by demonstration. Figures 21-24 demonstrate what happens to a random f(t). In the figures the numbers along the time axes refer to two hour intervals, so the total time is 3000 hours. Figure 21 shows a signal of 1500 random Gaussian numbers with zero mean and variance one. Figure 22 shows the result of transforming the random signal, setting to zero all coefficients corresponding to frequencies outside the range .0367 to .0467 cycles per hour , and then inverse transforming. In this case a = .01 cycles/hour and b = 1/24 cycles/hour. Notice the 24 hour oscillations introduced in Figure 22. Figure 23 does the same for a = .01 and b = 1/12.40. Figure 24 shows the results of using a = .02 and b = 1/12.40.

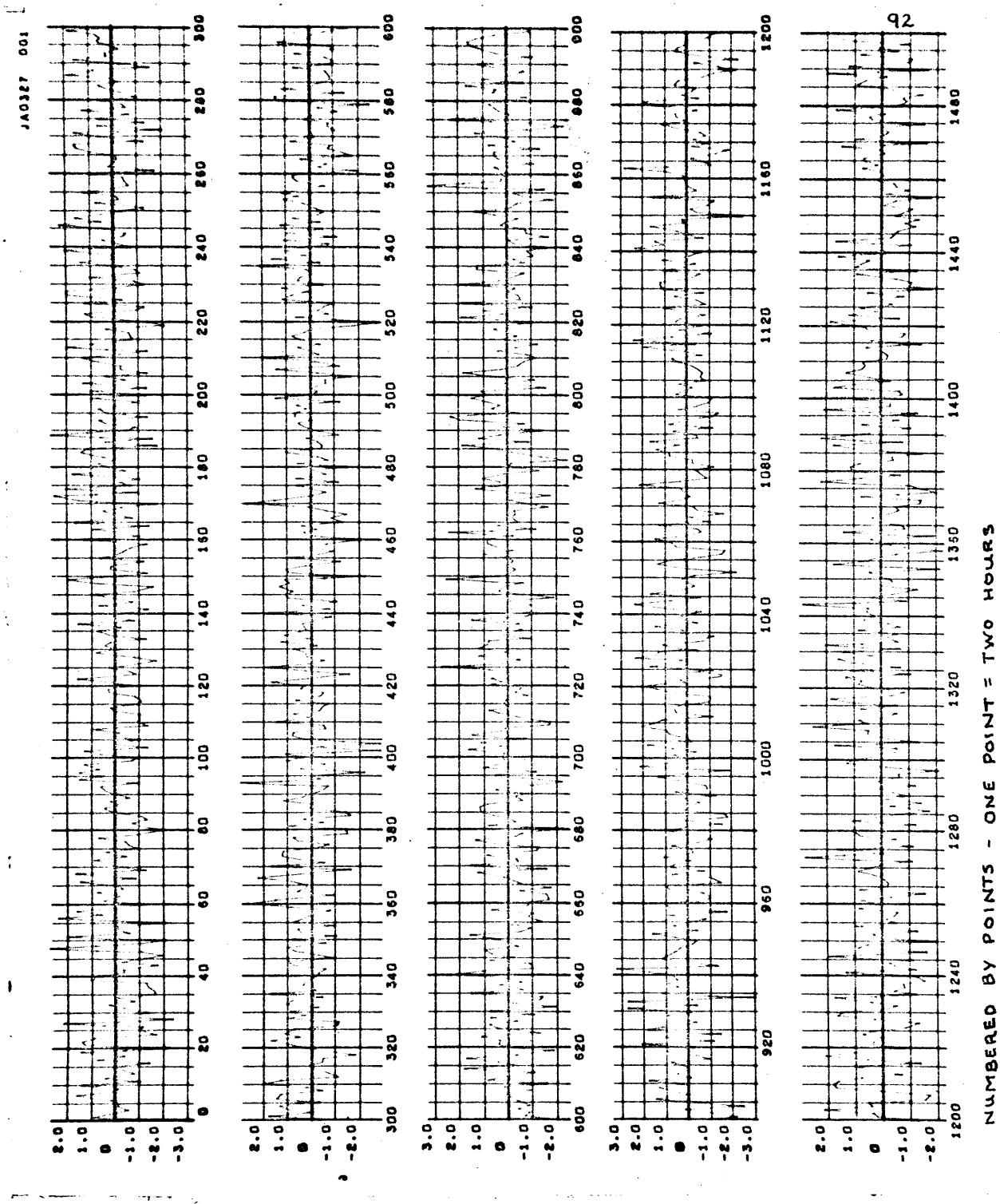

FIGURE 21

SIGNAL BEFORE BAND-PASSING

1500 RANDOM VALUES - ONE EVERY TWO HOURS

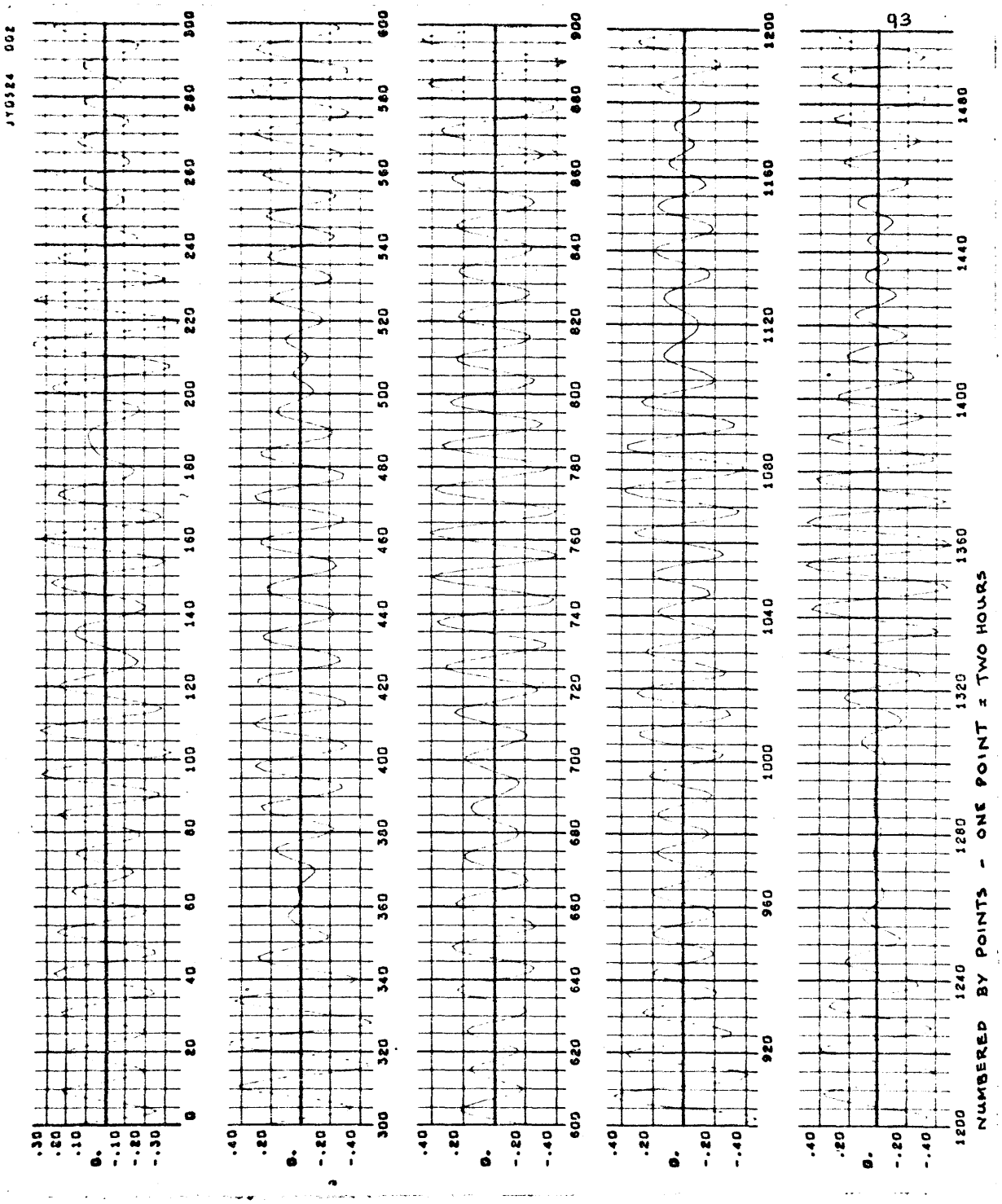

FIGURE 22

SIGNAL AFTER BAND-PASSING

BAND CENTERED AT 1/24 CY/HR. BANDWIDTH = .01 CY/HR.

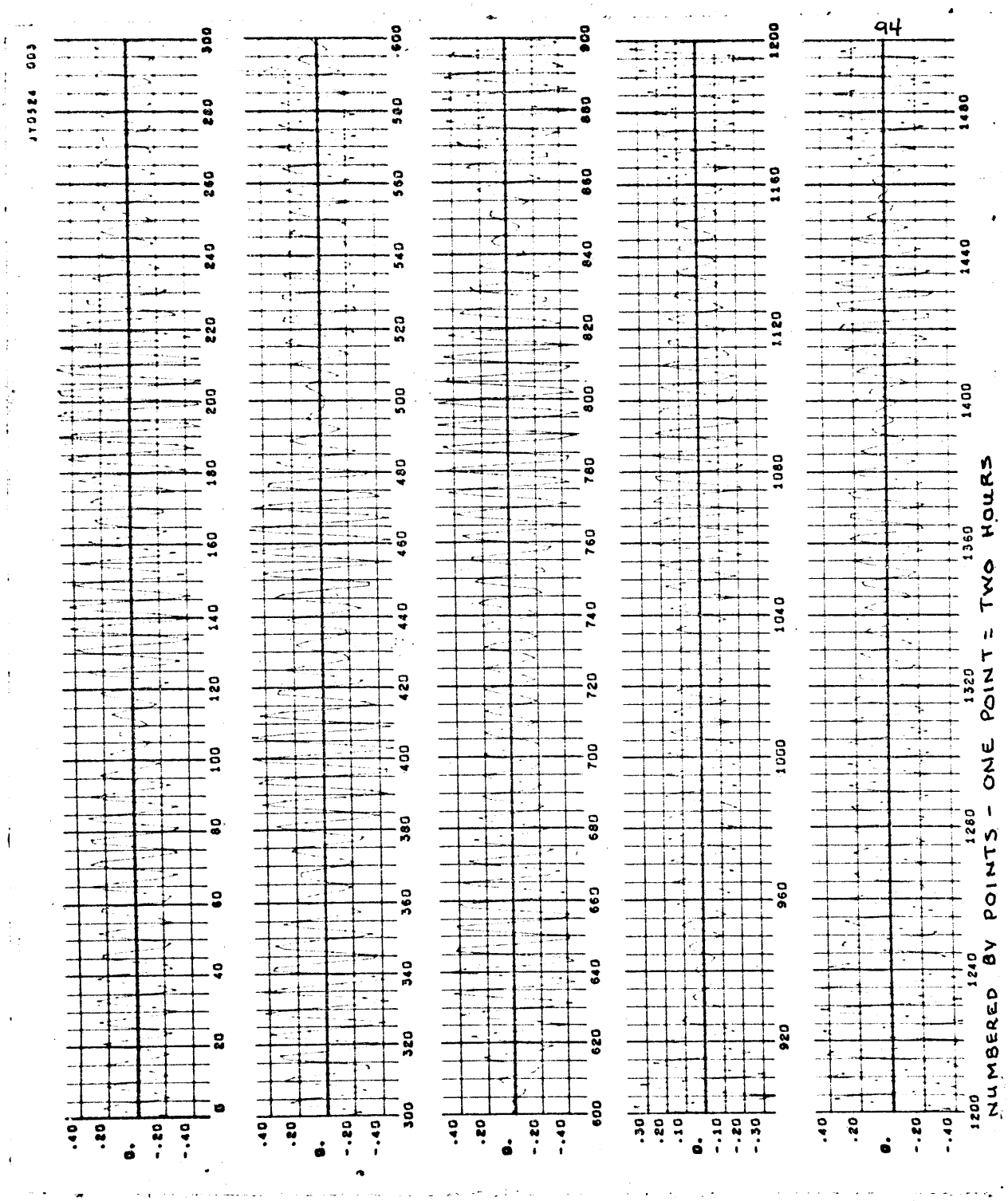

FIGURE 23

SIGNAL AFTER BAND-PASSING

BAND CENTERED AT 1/12.40 CY/HR. BANDWIDTH = .01 CY/HR.

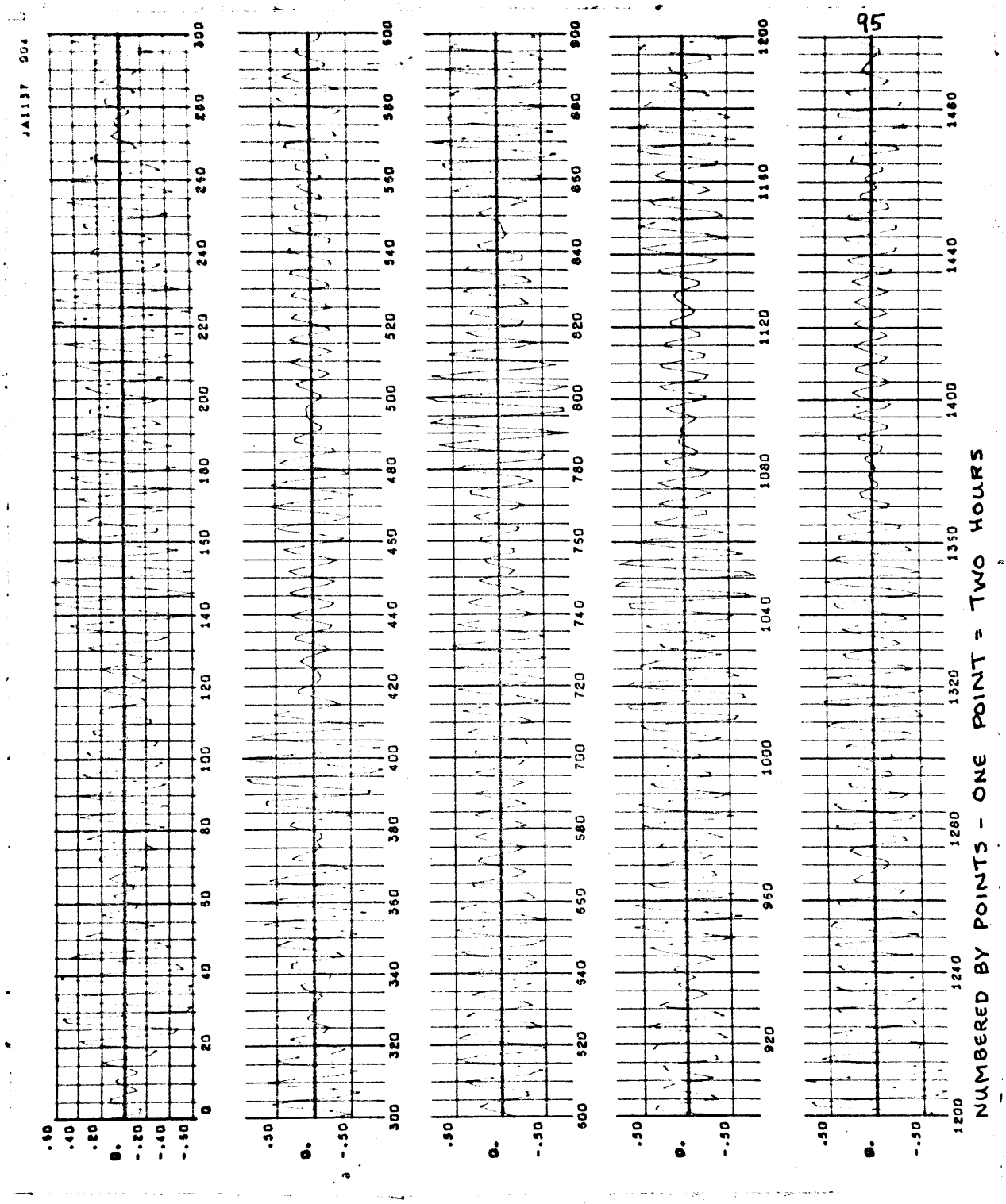

FIGURE 24

SIGNAL AFTER BAND-PASSING

BAND CENTERED AT 1/12.40 CY/HR. BANDWIDTH = .02 CY/HR.

REFERENCES

Bracewell, R., The Fourier Transform and Its Applications, 381 pp., McGraw Hill Book Company, New York, 1965.

Cox, C.S., and H. Sandstrom, Coupling of internal and surface waves in water of variable depth, Oceanog. Soc. Japan, J., 20th Aniversary Vol., 499- 513, 1962.

Defant, A., On the origin of internal tide waves in the open sea, J. Marine Res., 9(2), 111-119, 1950.

Defant, A., Ebb and Flow, 121 pp., University of Michigan Press, Ann Arbor, 1958.

Doebler, H.J., Savonius current measurements of deep ocean currents on the slope of Plantagenet Bank, Bermuda, J. Geophy. Res., 72(2), 511-519, 1967.

Doodson, A.T., and H.D. Warburg, Admiralty Manual of Tides, 270 pp., His Majesty's Stationery Office, London, 1941.

Fofonoff, N.P., Spectral characteristics of internal waves in the ocean, Deep-Sea Res., 16(supplement), 59-72, 1969.

Gerges, M.A., Variations of tidal currents measured at deep-sea moorings, p. 30, Scientific report, Department of Meteorology, Massachusetts Institute of Technology, Cambridge, Mass., 1966.

Gonella, J., Spectral analysis of vector series in two dimensions, Unpublished manuscript, 1971.

Hecht, A., and P. Hughes, Observations of temperature fluctuations in the upper layers of the Bay of Biscay, Deep-Sea Res., 18(7), 663-684, 1971.

Isaacs, J.D., J.L. Reid, Jr., G.B. Schick, and R.A. Schwartzlose, Near bottom currents measured in 4 kilometers depth off the Baja California coast, J. Geophys. Res., 71(8), 4297-4303, 1966.

Le Blond, P.H., On the damping of internal gravity waves in a continuously stratified ocean, J. Fluid Mech., 25(1), 121-142, 1966.

Lee, W.K.H., and C.S. Cox, Time variation of ocean temperatures and its relation to internal waves and oceanic heat flow measurements, J. Geophys. Res., 71(8), 2101-2111, 1966.

Middleton, D., Some general results in the theoty of noise through non-linear devices, Quart. Appl. Math., 5(4), 455-498, 1948.

Munk, W., and N. Phillips, Coherence and band structure of inertial motions in the sea, Rev. Geophys., 6(4), 447-472, 1968.

Niiler, P.P., On the internal tidal motions in the Florida Straights, Deep-Sea Res., 15(1), 113-123, 1968.

Nowroozi, A.A., M. Ewing, J.E. Nafe, and M. Fleigel, Deep ocean current and its correlation with the ocean tide off the coast of Northern California, J. Geophys. Res., 73(6), 1921-1932, 1968.

Perkins, H., Inertial oscillations in the Mediterranean, p. 49, Ph.D. thesis, Department of Meteorology, Massachusetts Institute of Technology, Cambridge, Mass., and the Woods Hole Oceanographic Institution, Woods Hole, Mass., 1970.

Rattray, M., Jr., On the coastal generation of internal tides, Tellus, 12(1), 54-62, 1960.

Rattray, M., Jr., J.G. Dworski, and P.E. Kovala, Generation of long internal waves at the continental slope, Deep-Sea Res., 16(supplement), 179-196, 1969.

Richardson, W.S., P.B. Stimson, and C.H. Wilkins, Current measurements from moored buoys, Deep-Sea Res., 10(4), 369-388, 1963.

Sabinin, K.D., and V.A. Shulepov, Some results of studies on internal waves in the tropical Atlantic, Akademiia Nauk SSSR, Bulletin, Atmospheric and Oceanic Physics Series, 6(2), 103-107, 1970, Translation of: Izvestiya, Atmospheric and Oceanic Physics, 6(2), 189-197, 1970 (AGU).

Schureman, P., A Manual of the Harmonic Analysis and Prediction of Tides, 416 pp., Government Printing Office, Washington, 1966.

Webster, F., Vertical profiles of horizontal ocean currents, Deep-Sea Res., 16(1), 85-98, 1969.

Wunsch, C., The long period tides, Rev. Geophys., 5(4), 447-475, 1967.

Wunsch, C., Progressive internal waves on slopes, J. Fluid Mech., 35(1), 131-144, 1969.

Wunsch, C., Preliminary results of internal wave measurements in the main thermocline at Bermuda, J. Geophys. Res., 75(30), 5899-5908, 1970.

Wunsch, C., Internal waves, Amer. Geophys. Union Trans., 52(6), 233-235, 1971.